Diploma Thesis

Development of a setup to measure pressure of expansion in a confined environment Application to concrete

submitted in satisfaction of the requirements for the degree
Diplom-Ingenieur
of the TU Wien, Faculty of Civil and Environmental Engineering

---

Diplomarbeit

Entwicklung einer Anlage zur Messung des Ausdehnungsdrucks in einer begrenzten Umgebung Anwendung an Beton

ausgeführt zum Zwecke der Erlangung des akademischen Grads
Diplom-Ingenieur
eingereicht an der TU Wien, Fakultät für Bau- und Umweltingenieurwesen

Robert Dulguerov, BSc

Matr.Nr.: 01608069

Betreuung: Dipl.-Ing. Dr.techn. **Johannes Kirnbauer**
Ass. Prof. Dr. **Teresa Liberto**, BSc MSc
Univ.Prof. **Agathe Robisson**, PhD
Institut für Institut für Werkstofftechnologie, Bauphysik und Bauökologie
Forschungsbereich Baustofflehre, Werkstofftechnologie
Technische Universität Wien
Karlsplatz 13/E201-01, 1040 Wien, Österreich

Wien, im September 2023

Kurzfassung

In dieser Masterarbeit widmen wir uns einer praktischen Herausforderung in der Bauindustrie: der Verwendung von recyceltem Beton. Der Schwerpunkt dieser Studie liegt auf der Entwicklung eines neuen experimentellen Aufbaus, um zu untersuchen, wie recycelter Beton unter bestimmten Bedingungen expandiert, ein Phänomen, das als *interner Sulfatangriff (ISA)* bekannt ist. Dieses Problem ist entscheidend, da es die Langlebigkeit von recyceltem Beton beeinflusst, dessen Zusammensetzung variiert.

Unsere Arbeit beinhaltet den Aufbau einer Vorrichtung, die es uns ermöglicht, den Expansionsdruck innerhalb von begrenztem Beton zu messen. Dabei konzentrieren wir uns speziell darauf, wie Sekundär-Ettringit, ein Mineral, das in gehärtetem Beton entsteht, zu dieser Expansion beiträgt. Wir führten Experimente durch, um zu verstehen, wie verschiedene Faktoren wie die Zusammensetzung des Betons, seine Aushärtungsbedingungen und seine Exposition gegenüber Sulfaten diese Expansion beeinflussen.

Das Ziel dieser Forschung ist es, besser zu verstehen, wie recycelter Beton im Laufe der Zeit verschlechtern kann, und dieses Wissen zu nutzen, um die Recyclingpraktiken in der Bauindustrie zu verbessern. Indem wir uns auf den experimentellen Prozess und den von uns erstellten Aufbau konzentrieren, streben wir danach, praktische Erkenntnisse zur Haltbarkeit und nachhaltigen Verwendung von recyceltem Beton beizutragen.

Abstract

In this master's thesis, we address a practical challenge in the construction industry: the use of recycled concrete. The key focus of this study is the development of a new experimental setup to investigate how recycled concrete expands under certain conditions, a phenomenon known as *internal sulfate attack (ISA)*. This issue is crucial because it affects the longevity of recycled concrete, which varies in composition.

Our work involves building a setup that allows us to measure the expansion pressure within confined concrete, specifically looking at how secondary ettringite, a mineral that forms in hardened concrete, contributes to this expansion. We conducted experiments to understand how different factors like the makeup of the concrete, how it is cured, and its exposure to sulfate affect this expansion.

The goal of this research is to better understand how recycled concrete can deteriorate over time and to use this knowledge to improve recycling practices in the construction industry. By focusing on the experimental process and the setup we created, we aim to contribute practical insights into the durability and sustainable use of recycled concrete.

Contents

Introduction

Concrete is one of the most widely used construction materials due to its strength, durability, and ability to be molded into various shapes, such as vertical and horizontal slabs, beams, pillars, and the like. It is made by combining cement, aggregates (e.g. sand and gravel), water, and sometimes additives (e.g. superplasticizer). Cement, serving as the binding agent in concrete, plays a crucial role in providing the material with its strength and stability [19].

However, despite its numerous advantages, concrete is not impervious to damage. Several factors can adversely affect its durability over time. Exposure to environmental conditions, such as freeze-thaw cycles, chloride ingress from saltwater or de-icing salts, carbonation, and *sulfate attack* can all contribute to the deterioration of concrete structures [27].

The increasing utilization of recycled concrete is primarily motivated by the environmental impact of construction materials. In the context of global challenges posed by climate change, there is a growing emphasis on the reduction of carbon emissions and waste minimization. Recycling concrete serves the dual purpose of diverting waste from landfills and mitigating the necessity for fresh concrete production, a substantial contributor to carbon emissions.

Nevertheless, the incorporation of recycled concrete presents several challenges. One of these pertains to the potential presence of contaminated aggregates from recycled concrete, which can affect the strength and durability of newly manufactured concrete that uses recycled materials. When incorporating aggregates from older concrete into new concrete, they may be tainted by impurities or exhibit an elevated water absorption capacity. This susceptibility can result in issues such as increased shrinkage, diminished strength, and even the development of cracks in the new concrete [30].

Additionally, recycled concrete can contain sulfate-bearing aggregates, admixtures, and cementitious materials that can pose a significant problem for the concrete structure. Sulfates can also get into the concrete from external sources, such as ground and surface waters. These sulfate-rich solutions react with the calcium-aluminate hydrates, producing calcium sulfoaluminate. This reaction results in the formation of secondary ettringite, a hydration product that forms during the hydration of cementitious materials, once the concrete is set, which can cause the concrete to expand and crack, due to its needlelike crystalline structure [7].

This thesis explores *sulfate attack* on concrete structures and the creation of a specialized setup for measuring expansion pressures. It is structured as follows:

In chapter 1 we provide the background information that is relevant to understanding the content of the thesis. We review the chemistry of *sulfate attack*. Also, we underscore the factors that influence expansion due to *sulfate attack*, including sulfate concentration, temperature, and pH levels. Additionally, in this chapter, we discuss prior studies on *sulfate attack*, serving as the background information for this research. Furthermore, we outline the motivation behind and the methodology employed in this study, explaining why this research is significant and the approach taken for conducting the experiments.

In chapter 2 we delve into the materials used in the experiments. We provide insights into fresh cement, specifically two types, Der Blaue and SupraCem45. Hydrated cement, gypsum, and various additives are also introduced and discussed in detail. These materials constitute essential components for the investigation of sulfate attack and expansion in a confined environment.

In chapter 3 we outline the experimental methods and procedures used in this study. We begin by introducing the glass ampoule-breaking test, a premilitary method employed for these experiments, and then detail setup #1 for the experiments, highlighting the initial challenges encountered and the subsequent development of setup #2. Moreover, we provide an overview of the procedures for setting up the samples.

In chapter 4 we present the core findings of this study. This chapter includes the results of the glass ampoule-breaking experiment and the expansion in a confined environment experiment. We examine specific tests and experiments, such as Test 2.5 (SupraCem45 + hydrated gypsum + magnesium oxide), Test 2.6 (Der Blaue + hydrated gypsum), and Test 2.7 (Hydrated Der Blaue + hydrated Fondu + hydrated gypsum). Furthermore, we scrutinize the expansion behavior of different cementitious materials and compositions. A discussion accompanies the results, offering insights into the implications and significance of the findings.

In chapter 5 we provide a summary of the research findings and offer a perspective on the contribution of this research and potential avenues for further studies.

Chapter 1

State of the art

This chapter provides an overview of the principles of expansion in a confined area and the current state of the art in sulfate attack research, delving into the chemistry, influencing factors for expansion, and relevant studies that form the foundation for the motivation and methodology of the present study.

1.1 Expansion in a confined area

The understanding of material expansion in confined environments, particularly for cementitious materials such as concrete, has been a subject of significant interest in materials science and construction engineering. The expansion characteristics of materials like clay and concrete under restricted conditions have profound implications on the design and longevity of structures [18, 22].

The phenomenon of swelling in clays, as explored in Madsen's 1989 study [22], provides foundational insights into the expansion behavior of materials. Madsen's research delves into the interaction between environmental factors, notably moisture content, and the swelling properties of clay. This relationship is particularly relevant for cementitious materials, as both clay and cement share similarities in their response to moisture and compaction.

Building upon this understanding, Katti's 2001 study [18] on the swelling pressure of clay further shows the dynamics of expansion under confinement. This research highlights the critical role of moisture content and its direct correlation with the exerted swelling pressure in confined environments.

In the context of this study, the experimental setup needs to be engineered to measure the pressure generated by the expansion of cementitious materials within a confined environment. The primary aim is to recreate scenarios where cement samples are subjected to constrained expansion, reflecting real-world applications but within a controlled and accelerated testing environment. A simple schematic of a swelling cell used in the study of Katti in 2001 is shown in fig. 1.1 [18]. This setup will be the first point of reference for the construction of the setup that will be used for this study since the conducted experiments are similar.

The confinement chamber needs to be designed to restrict the expansion of cement samples while allowing for measurement of the exerted pressure. This chamber emulates the physical restrictions encountered by materials in construction settings, where expansion is often limited by the hardened structure.

Temperature and moisture control mechanisms within the setup are important, considering their established impact on material expansion. Drawing from the findings in Madsen's and Katti's studies [18, 22], these controls allow for the simulation of various environmental conditions, thereby enabling an analysis of how these factors influence the expansion pressure of concrete.

The application of this setup to concrete is particularly relevant in understanding scenarios such as moisture-induced swelling or chemical expansion, common challenges in the construction industry. In this study we focus on the chemical expansion due to *sulfate attack*.

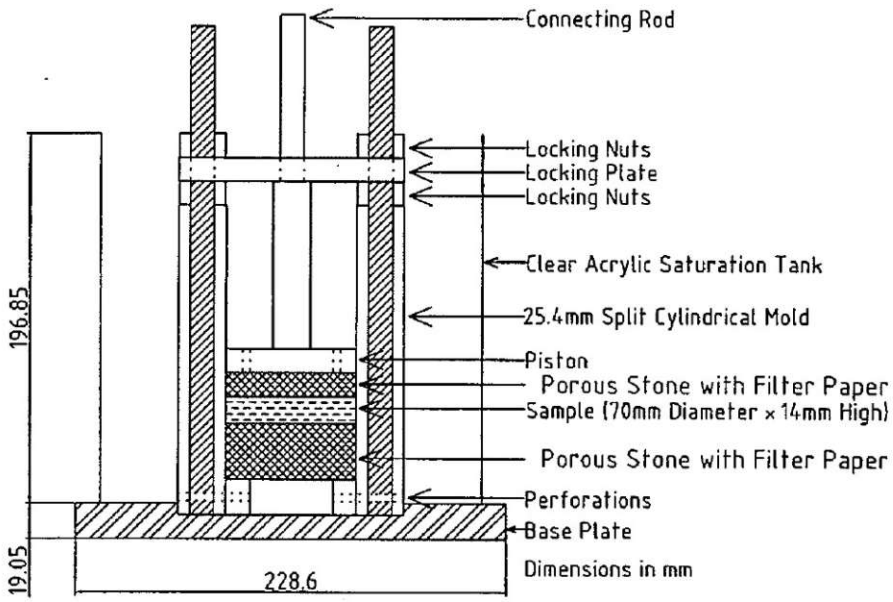

Fig. 1.1: Schematic illustration of the controlled uniaxial swelling cell [18]

1.2 *Sulfate attack*

Sulfate attack is a well-known phenomenon that can lead to the degradation of concrete structures. It is characterized by the expansion of the concrete due to the formation of ettringite in the pores [6]. Ettringite is a hydration product that forms in cement mixtures. The main component of cement is Portland cement clinker, which is composed of calcium silicates. When water is added to cement, a series of chemical reactions take place, leading to the reaction of tricalcium aluminate with sulfate ions present in the mixture. Ettringite crystals form and those may lead to the expansion of the material. There are two main types of ettringite formations: primary ettringite and secondary ettringite [2]. Primary ettringite is formed during the initial stages of cement hydration. It typically occurs within the first 24 hours after mixing cement with water. The rapid formation of primary ettringite can be influenced by factors such as high levels of sulfate in the water and elevated temperatures during the early stages of concrete curing. Secondary ettringite forms at later stages in the life of concrete, typically after several days or weeks. It can result from the uptake of sulfate from external or internal sources, such as the surrounding environment or aggregates used in the concrete mix. Specifically, when recycled concrete is used, sulfate might be present in the mixture. Overall, the formation of ettringite in the hardened material pores creates tensile pressure, which can lead to the formation of cracks when the pressure exceeds the tensile strength of the samples [2].

The relationship between the quantity of ettringite produced and the subsequent expansion is observable in shrinkage-compensating cement [16]. This type of cement incorporates a blend of ingredients including aluminum-rich cement (e.g. calcium aluminum cement), standard Portland cement, and gypsum. The additional expansion is a consequence of increased secondary ettringite formation and serves as compensation for shrinkage induced by factors such as water diffusion into the soil, or chemical and autogenous shrinkage [9, 16]. The extent of expansion is directly proportional to the quantity of gypsum present, as demonstrated by research findings. For example, the addition of 15% gypsum to a cement paste results in a linear expansion of 175% [9, 29].

The occurrence of *sulfate attack* can be classified based on two different processes or the specific location where it occurs, encompassing both physical and chemical interactions as well as external and internal factors.

Physical sulfate attack (PSA) involves a recurring process of sulfate salt crystal formation and decomposition, as well as ettringite formation, within the inner structure of cement paste or concrete [28]. This phenomenon eventually leads to fatigue-induced degradation [25, 44]. When sodium sulfate is the aggressive agent, it triggers the dissolution and precipitation of salts within the concrete, resulting in occurrences such as efflorescence and sub-florescence. In regions adjacent to the sea or rich in sulfate sources, these salts infiltrate the pores of permeable concrete. As water evaporates, the salt concentration becomes supersaturated, causing recrystallization within the concrete pores. The resultant crystallization pressure can exceed the concrete tensile strength, leading to crack formation [26, 35]. The influence of temperature and humidity fluctuations within the concrete plays a significant role in *PSA*.

Conversely, *chemical sulfate attack (CSA)* arises from chemical reactions between cement clinker phases (particularly tricalcium aluminate C_3A) or cement hydration products (such as calcium hydroxide and monosulfate) and sulfate ions. These reactions give rise to the formation of ettringite or gypsum under specific conditions (see section 1.3 for reactions), leading to expansion and gradual deterioration of the concrete. These chemical reactions commence during the cement-water mixing process and persist throughout the concrete lifespan [28, 35].

In the context of damage to concrete structures, it is important to determine where the sulfate attack takes place. *External sulfate attack (ESA)* occurs when sulfate ions from external solutions cause expansion of the material causing surface damage to the concrete. *Internal sulfate attack (ISA)*, on the other hand, involves the reaction of sulfates from within the material to form secondary ettringite. This ettringite can later decompose and lead to the release of sulfate ions, causing homogeneous expansion in the concrete and deteriorating it from within [7].

To mitigate the effects of *CSA* and *PSA* in concrete, several actions can be implemented [28, 48]:

- Reduce the *water-to-cement ratio (w/c)*: lowering the *w/c* ratio helps reduce the permeability of concrete, making it less susceptible to sulfate ion diffusion and minimizing the potential for *sulfate attack*.
- Use C_3A-free cement or cement with minimum aluminate content: C_3A (tricalcium aluminate) is a component of cement that can react with sulfates, leading to detrimental expansive reactions. Using C_3A-free cement or cement with low C_3A content can minimize the risk of *sulfate attack*.
- Improve concrete compaction: denser compaction and lower porosity of concrete can be disadvantageous in resisting expansive reactions caused by ettringite formation in *ISA*. However, proper compaction techniques can still be employed to enhance the overall durability and strength of the concrete.
- Implement surface finishing: the use of surface finishes can help minimize sulfate ion diffusion into the concrete, reducing the potential for physical *sulfate attack* and the formation of sulfate salt crystals.

1.3 Chemistry of *sulfate attack*

The chemistry of *sulfate attack* on concrete involves a series of intricate reactions that ultimately affect the integrity of the concrete structure. Starting with the reaction of sulfate ions (SO_4^{2-})

with calcium cations (Ca^{2+}), leading to the formation of gypsum, $CaSO_4{\cdot}2H_2O$ as shown in (equation 1.1). This initial reaction marks the starting point of *sulfate attack* [3, 28, 31].

Subsequently, gypsum engages in further chemical reactions within the cement paste. When gypsum encounters unhydrated C_3A, it initiates the formation of early or primary ettringite (reaction (1.2)). This crucial step occurs within the first 24 hours after mixing the cement. Importantly, during this timeframe, the cement paste remains deformable and has not yet hardened, thus the formation of primary ettringite is generally considered non-harmful and does not lead to significant expansion ($(\Delta\nu = 0\%)$) [23, 24, 41].

However, when gypsum becomes scarce, early ettringite can react with any remaining unhydrated C_3A to produce monosulfate, following a distinct chemical equation 1.3. Monosulfate is an unstable phase and can transform into secondary ettringite when sulfate and calcium ions become available, as outlined in the chemical equation 1.4. This transformation results in substantial volumetric changes, with 1 mole of ettringite formed from this process causing a significant expansion ($\Delta\nu = 2.48 * 10^{-4} \frac{m^3}{mol}$) [31].

Furthermore, secondary ettringite can also form through the reaction of the remaining unreactive C_3A with calcium hydroxide (a hydration product from C_3S), water, and sulfate ions. This reaction is known to cause expansion, further complicating the concrete stability ($\Delta\nu = 3.94 * 10^{-4} \frac{m^3}{mol}$) [31].

The formation of secondary ettringite, as seen in reactions 1.4 and 1.5, typically occurs in substantially hardened concrete [41]. Notably, the transformation of 1 mole of C_3A into 1 mole of ettringite is associated with approximately an 8-fold increase in volume, underscoring the magnitude of the expansion process [3]. Interestingly, this delayed ettringite formation can occur months to even years after the initial casting of the concrete, highlighting the long-term implications of *sulfate attack* and with its expansion [32, 41].

The molar ratio of $CaSO_4{\cdot}H_2O/C_3A$ plays a critical role in determining which hydration products, such as ettringite or monosulfate, will ultimately form, adding complexity to the chemical dynamics of *sulfate attack* on concrete [31].

$$Ca^{2+} + SO_4^{2-} + 2H_2O \longrightarrow CaSO_4 \cdot 2H_2O + 2(OH)^- \tag{1.1}$$

$$C_3A + 3CaSO_4 \cdot 2H_2O + 26H_2O \longrightarrow C_3A \cdot 3CaSO_4 \cdot 32H_2O \tag{1.2}$$

$$C_3A \cdot 3CaSO_4 \cdot 32H_2O + 2C_3A + 4H_2O \longrightarrow C_3A \cdot CaSO_4.12H_2O \tag{1.3}$$

$$C_3A{\cdot}CaSO_4{\cdot}12H_2O + 2Ca(OH)_2 + 20H_2O + SO_4^{2-} \longrightarrow C_3A{\cdot}3CaSO_4{\cdot}32H_2O + 4(OH)^- \tag{1.4}$$

$$C_3A + 3Ca(OH)_2 + 26H_2O + 3SO_4^{2-} \longrightarrow C_3A \cdot 3CaSO_4 \cdot 32H_2O \tag{1.5}$$

$CaSO_4 \cdot H_2O$ = gypsum

$CaSO_4$ = calcium sulfate

$C_3A \cdot 3CaSO_4 \cdot 32H_2O$ = ettringite

$C_3A \cdot CaSO_4 \cdot 12H_2O$ = calcium aluminate monosulfate hydrate

$C_3A = 3CaO \cdot Al_2O_3$ = tricalcium aluminate

$C = CaO_2$ = calcium peroxide

$S = SiO_2$ = silicon dioxide

$A = Al_2O_3$ = aluminum oxide

$M = MgO$ = magnesium oxide

$\bar{S} = SO_3$ = sulfur trioxide

$H = H_2O$ = water

1.4 Influencing factors for expansion due to *sulfate attack*

This section delves into the critical factors that influence *sulfate attack* on concrete. As already mentioned, *sulfate attack* is a complex process with significant implications for concrete durability, shaped by various factors, including sulfate ions, temperature fluctuations, pH levels, and other key parameters affecting the concrete response to corrosive process [31, 36, 47]. Sulfate ions are at the heart of *sulfate attack* and understanding their behavior within the concrete matrix is important for effective *sulfate attack* management [31]. Temperature variations play a role in this context. Concrete undergoes both high and low-temperature exposures during its lifecycle, impacting its reaction to sulfate ions [36]. The pH levels are indicators of environmental acidity or alkalinity and also have an impact on the process of *sulfate attack*. They dictate the dissolution or stability of specific concrete compounds, including gypsum and sulfates [47].

1.4.1 Sulfate

Gypsum is typically added in small quantities to clinker (approximately 5% of the final cement amount) and plays a crucial role in cement production. This addition occurs either during or after the milling of clinker and serves multiple purposes [11]. Firstly, gypsum enhances the contact area for milling of the clinker during the process, contributing to the presence of finer particles. Gypsum is easier to mill than clinker, which leads to a more finely ground product. Secondly, and perhaps more importantly, gypsum acts as a retarder, preventing the rapid hardening of the clinker phase C_3A when it comes into contact with water. This initial delay in setting is vital because if C_3A were to react rapidly and solely with water in the absence of sulfate, it would lead to the formation of unstable phases such as C_2AH_8 and C_4AH_{19}, which would eventually transform into the more stable hydrogarnet phase C_3AH_{60}. These intermediate phases are notorious for causing flash setting, which significantly reduces the available time for the placement and compaction of concrete. Furthermore, they hinder the complete hydration process of cement phases. [14, 17, 31].

However, when sulfate is introduced into the system, a different scenario unfolds. The presence of sulfate ions leads to the formation of primary ettringite (shown in section 1.3 ($C_3A \cdot 3\ CaSO_4 \cdot 32\ H_2O$), which coats the C_3A particles with a protective ettringite layer. This layer acts as a barrier, preventing further hydration of C_3A with water. As a result, the concrete maintains adequate workability, allowing it to be properly placed and compacted. This critical role of sulfate in forming primary ettringite helps ensure concrete workability [14, 17, 31].

It is important to categorize the severity of sulfate attacks based on the solubility of sulfate ions in soil or groundwater (see tab.1.1). A categorization based on internal sulfate ions due to the incorporation of recycled concrete has yet to be made. Concrete design must then consider factors such as water-cement ratio, minimum compressive strength, the incorporation of supplementary

cementitious materials, and minimum air content, all tailored to the specific sulfate exposure conditions. This approach ensures that concrete structures are built to withstand the challenges posed by varying sulfate levels, whether the exposure is moderate, severe, or very severe [26].

degree of exposure	water-soluble sulfate in soil [%]	sulfate in groundwater [mg/L]	min. 56-Day compr. strength [MPa]	max. w/b ratio [-]	cem. material to be used
moderate	0.1-0.2	150-1,500	30	0.50	20E, 40 or 50E
severe	0.2-2.0	1,500-10,000	32	0.45	50t
very severe	over 2.0	over 10,000	35	0.40	50t

Tab. 1.1: Severity of *sulfate attack* and the requirement of concrete based on the exposure condition [26] (adapted from the Canadian standard A23.1)

1.4.2 Temperature

The role of temperature in *sulfate attack* on concrete is a factor that can significantly influence the behavior and durability of the material. Concrete undergoes various temperature conditions during its lifecycle, and these can have profound effects on its properties and susceptibility to *sulfate attack* [33]. Concrete can be exposed to elevated temperatures during hydration and curing processes. For example, precast concrete may be subjected to steaming or heat curing at temperatures ranging from 60-70°C. This elevated temperature is employed to accelerate the initial compressive strength development and facilitate the demolding process or prestressing at early stages [8]. However, an increase in temperature, particularly above 70°C, can result in significant consequences. At such high temperatures, the water in the concrete can partially evaporate which leads to an increase in the overall porosity of the concrete. This can hinder the complete hydration of cement phases due to reduced water availability, leading to a decrease in concrete strength. Furthermore, the increased porosity and slow rate of hydration can make the concrete more vulnerable to deterioration and surface cracking [33]. Additionally, the presence of cracks can facilitate the easier diffusion of sulfate into the concrete due to increased permeability [8].

When concrete has been exposed to high curing temperatures above 70°C it is subsequently stored in water at lower temperatures (around 20°C) and it can experience the dissolution of ettringite [7]. Conditions that encourage this delayed formation of ettringite include a sulfate-to-aluminate ratio (SO_4^{2-}/Al^{3+}) above 0.5 [26]. Inversely, lower temperatures in the range of 10-20°C can lead to the formation of thaumasite, a calcium sulfosilicate compound ($CaSiO_3 \cdot CaCO_3 \cdot CaSO_4 \cdot 15H_2O$), and can result in the decomposition of *calcium silicate hydrates (C-S-H)* [36, 38], the main hydration product of concrete responsible for its strength and durability [7]. This phenomenon can cause the concrete to soften and experience a loss in strength [36]. The formation of thaumasite requires the presence of both calcium sulfate and a source of carbonate ions. These carbonate sources can originate from concrete exposure to air and subsequent carbonation or from cement containing limestone added during production or milling [26, 36, 38].

1.4.3 pH Level

The role of pH level in *sulfate attack* on concrete is a factor that can affect the behavior and durability of the material [21]. The pH, a measure of the acidity or alkalinity of a solution, plays a role in regulating the chemical reactions that take place in the concrete matrix when exposed to sulfate ions.

The pH level of the environment determines the availability of hydrogen ions (H^+) in the solution. In acidic conditions (low pH), hydrogen ions are abundant, which can promote the dissolution of calcium-based compounds in the concrete matrix. This dissolution can lead to the breakdown of the cementitious structure and result in the loss of strength and integrity of the concrete [47].

On the other hand, in alkaline conditions (high pH), the presence of hydroxide ions (OH^-) dominates the solution. Alkaline conditions can favor the formation of stable *C-S-H* and other cementitious phases, protecting against *sulfate attack*. However, extreme alkalinity can also lead to the transformation of ettringite into more stable phases, particularly monosulfate and/or monosulfoaluminate. These phases lead to volume expansion in hardened concrete and therefore loss of durability [21].

Achieving the right pH balance impacts *sulfate attack* on concrete. Factors such as the initial mix design, cement composition, and the exposure environment have to be considered to control the pH levels. Additionally, supplementary cementitious materials, like fly ash or slag, can be added to concrete mixtures to help maintain a more stable pH range, reducing the susceptibility to *sulfate attack* [21, 47].

1.5 Studies on *sulfate attack*

Studies on *sulfate attack* have encompassed a range of methodologies designed to understand and accelerate the complex deterioration processes. One key aspect of these investigations is the recognition that the formation of secondary ettringite is the primary contributor to concrete degradation and can occur over extended periods, spanning several months to even decades after casting [27, 32, 41].

In an attempt to better understand *sulfate attack*, scientists have primarily tried to accelerate the formation of secondary ettringite [10, 20, 43, 45]. To expedite these reactions, two prominent methods have been employed. Firstly, exposing concrete to solutions with elevated sulfate concentrations serves as an effective means of acceleration. The rate at which sulfate penetrates the concrete, driven by factors such as permeability, dictates the timeline of degradation. Secondly, subjecting concrete or cement paste samples to weathering cycles, involving alternations between drying and wetting or variations in temperature and humidity simulates the effects of environmental conditions on deterioration. The wetting cycles involve partial or complete submersion in water or sulfate-rich solutions at ambient temperatures, followed by drying cycles at elevated temperatures [20, 45].

For instance, in the work of Xie and colleagues, concrete samples underwent drying/wetting cycles and exposure to varying concentrations of sodium sulfate solution [46]. These samples were either fully or partially immersed in sulfate solution at 23°C for three days, followed by drying cycles at 45°C over 40 weeks. Notably, fully submerged concrete exhibited minimal deterioration as it primarily underwent chemical attack. In contrast, concrete subjected to drying/wetting cycles, especially under partial submersion conditions, displayed heightened deterioration due to the combination of both chemical and physical *sulfate attack* [46].

Similarly, Wang investigated the impact of drying/wetting cycles on concrete deterioration, positing that these cycles facilitate sulfate ion penetration through capillary forces in addition to conventional diffusion and penetration [44]. This enhanced sulfate penetration promotes the precipitation of hydration products within concrete pores, culminating in strength augmentation. However, the subsequent drying phase induces supersaturation and salt crystal precipitation, exerting pressure on pore walls, leading to expansion and eventual deterioration [44].

Numerous experimental works have employed combinations of weathering cycles (representing *physical sulfate attack*) and exposure to high sulfate concentrations (i.e. *chemical sulfate attack*) over periods ranging from six months to one or two years [10, 20, 43, 45]. These studies focus on enhancing damage by increasing concrete permeability, with methodologies encompassing assessments of changes in cement microstructure, elastic modulus, quantification of hydration products through X-ray diffraction (XRD), expansion measurements, and weight changes [10, 20, 43, 45].

Notably, one of the longest-lasting studies on *sulfate attack* spanned 40 years, initiated by the American Bureau of Reclamation in 1940 [27]. This extensive investigation explored the impact of factors such as water to cement *w/c ratio*, the addition of pozzolanic materials, and the composition of C_3A and C_3S in cement. It was observed that the *w/c ratio* played a decisive role in determining sample failure. Samples with *w/c ratios* less than 0.45 exhibited no failure (defined as expansion exceeding 0.5%) over the entire 40-year duration, regardless of C_3A content. This indicated that such samples had extremely low permeability, restricting sulfate diffusion and subsequent expansion. The amount of C_3A in cement also significantly influenced the onset of expansion and deterioration, particularly when combined with higher *w/c ratios*. An increased C_3A content, as well as higher C_3S content, accelerated deterioration due to mechanisms involving ettringite and gypsum formation, as well as *C-S-H* decomposition [27].

A commonly employed methodology in *sulfate attack* studies is the measurement of expansion at intervals over time. Concrete prisms are prepared, and changes in length are recorded to track expansion progression [36]. Weight change over time can also indicate the formation of new hydration products, contributing to an increase in weight [7]. Conversely, weight loss signals deterioration, such as scaling or leaching.

Furthermore, comprehensive assessments often include measurements of compressive strength and modulus of elasticity evolution over time [40], scanning electron microscopy (SEM) to analyze microstructure changes, XRD for quantifying crystalline hydration products, calorimetry tests to monitor reaction heat evolution associated with new hydration product formation, chemical titration to quantify sulfate concentration, X-ray spectroscopy to correlate microstructural changes observed through SEM with damaging products [51], plasma spectrometry to measure cation leaching [5], energy dispersive spectroscopy to gauge molar ratios of products observed via SEM [49], and Mercury intrusion porosimetry to assess pore structure following *sulfate attack* [44, 46, 49]. Additionally, ultrasonic wave measurements are employed to track changes in dynamic modulus of elasticity in scenarios involving drying and wetting cycles [49].

These diverse methodologies form the foundation of our understanding of *sulfate attack*, enabling researchers to gain comprehensive insights into the complex processes governing concrete deterioration over time.

1.6 Motivation and methodology for this study

The motivation behind this study is to address critical challenges in the construction industry, particularly in the context of recycling concrete, which holds significant economic and ecological importance. The production of cement, a fundamental component in construction, heavily relies on finite natural resources, and its continuous production significantly depletes these resources [30]. Furthermore, the carbon dioxide (CO_2) emissions associated with cement production constitute a major contributor to environmental contamination and climate change. As such, the recycling of concrete waste and its integration into the construction industry represents a sustainable and ecologically responsible practice that promises both economic and environmental benefits [30, 46].

The realm of *sulfate attack* in concrete, characterized by its intricate physical chemistry, has spurred extensive research efforts. However, much of this research has predominantly focused on *ESA*, leading to a body of knowledge marked by occasional contradictions and contentious interpretations [28]. In contrast, *ISA* remains a comparatively underexplored territory within the domain of *sulfate attack*, necessitating further investigations to understand its mechanisms of deterioration. *ISA* has particular significance in the context of recycled concrete, as concrete waste materials may contain sulfates, as already mentioned. Factors such as the original quantity of C_3A, aluminum content, presence of ettringite and AFm (aluminate ferrite monosubstituted) phases, and initial gypsum or sulfate content are important determinants of structural safety and long-term durability [46, 50].

One important aspect of research on *sulfate attack* on concrete is the gradual formation of secondary ettringite within well-hardened concrete structures over several years. This extended process provides valuable insights into how concrete deteriorates due to sulfate exposure. What adds to its interest is that this expansion occurs within the confined spaces of the concrete, leading to its deterioration. Understanding the amount of pressure generated by this expansion within this enclosed environment is the first step to understanding concrete degradation process due to *sulfate attack*.

To measure the expansion pressure caused by secondary ettringite, a series of controlled experiments are conducted. These experiments utilize specific conditions that accelerate the process, making it easier and faster to measure the occurring pressure. By subjecting concrete samples to these controlled conditions that expedite *sulfate attack*, and closely monitoring their reaction, critical information about the pressure exerted by secondary ettringite is obtained. This data helps quantify the expansion pressure and its relationship with factors like concrete composition, curing conditions, and sulfate exposure.

This research builds upon preliminary studies by Hossam Al Daffaie, whose master thesis on *Expansion phenomena during sulfate attacks* highlighted the limited knowledge on *ISA* and the issues related to its expansive behavior [1]. In pursuit of investigating the expansion pressure generated by secondary ettringite formation and its impact on concrete deterioration, a dedicated experimental setup was designed and constructed. This setup was tailored to meet the specific requirements essential for this study. To accelerate the *sulfate attack* process and facilitate the measurement of occurring pressure, concrete specimens were subjected to controlled conditions designed to expedite the reaction. These specimens were allowed to react for a duration of up to 28 days, enabling the collection of data regarding expansion pressure and its evolution over time. Challenges related to the setup included the need for a very stiff confined area to prevent expansion, continuous contact of the sample with water, and prolonged heating to accelerate the sulfate attack process. Additionally, precise measurement of the force exerted by the sample over extended periods was important to gather accurate data on the evolution of expansion pressure.

Chapter 2

Material

The core materials used in this study were different types of cement, including the aluminium-rich *Fondu* cement, the conventional Portland cement known as *Der Blaue*, the exceptionally fast-setting Schretter *SupraCem 45* cement, and the sulfate-resistant *Contragress* cement. Each of these cementitious agents carries unique attributes that can significantly impact the performance of concrete mixtures. Furthermore, an investigation into the hydrated forms of these types of cement is conducted, simulating the conditions of recycled concrete. Gypsum, and a selection of additives, including calcium oxide to accelerate reactions, and magnesium oxide to enhance sample swelling, are also introduced.

2.1 Fresh cement

2.1.1 *Der Blaue*

Ordinary Portland cement, commonly referred to as *Der Blaue* [15] is one of the most widely used cement in Austria. This cement variant is categorized as *Der Blaue* CEM I 52.5 R, signifying its classification as a high-performance cement [15]. Its particle size distribution analysis measuring via the Mastersizer 3000: a D10 value of 3.1 μm, a D50 value of 13.5 μm, and a D90 value of 38.4 μm (fig. 2.1). *Der Blaue* composition primarily comprises four main clinker phases: C_3S, C_2S, C_3A, and C_4AF. Among these, C_3S is of importance, as it plays a role in the strength development of the cement through hydration with water, subsequently leading to the precipitation of compounds like C-S-H and Portlandite (CH). The C_2S phase, on the other hand, contributes to the gradual strength gain of the cement paste. To regulate the reactivity of C_3A with water, a small amount of gypsum (approximately 5%) is already incorporated into the cement mix. This addition prevents the rapid reaction of C_3A upon contact with water, preserving workability as mentioned in the chapter 1 section 1.2 [14, 39].

However, it is worth noting that *Der Blaue* cement exhibits low resistance to *sulfate attack*, making it unsuitable for use in environments with high levels of sulfate contamination[14, 39].

2.1.2 SupraCem45

Schretter SupraCem45 [37] is a hydraulic and fast-hardening binder. This binder is derived from Portland cement clinker, finely ground in conjunction with calcium sulfate, i.e. unhydrated gypsum. *SupraCem45* has high early and final strength characteristics due to its composition. To control the setting time of the cement, adjustments are made by incorporating setting retarders like tartaric acid into the mortar recipe [37].

This fast-setting mortar derives its rapid-setting attributes from a chemical process within the cement paste. The incorporation of Al^{3+}-ions triggers an immediate conversion into $Al(OH)^{4-}$-ions due to the alkaline environment of the cement paste. These $Al(OH)^{4-}$-ions subsequently start

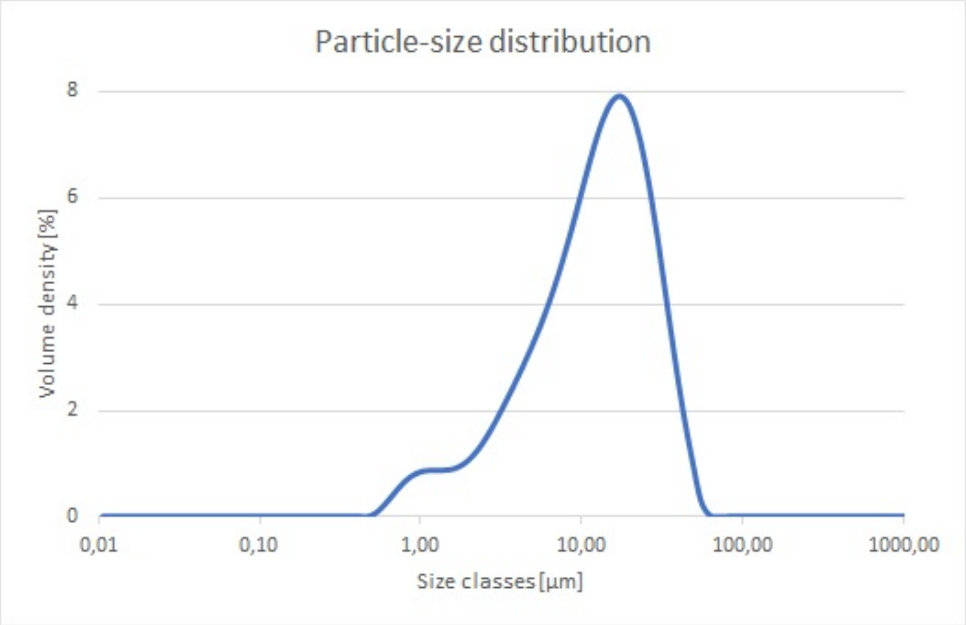

Fig. 2.1: Particle-size distribution of cement *Der Blaue*

a chemical reaction with SO_4^{2-}—ions in conjunction with Ca^{2+}-ions. This intricate chemical reaction leads to the formation of ettringite, the primary factor responsible for expediting the setting process. Notably this ettringite formation leads to rapid expansion [4] as fully explored in chapter 1 section 1.3.

A particle size distribution analysis using the Mastersizer 3000 was measured again, providing a D10 value of 3.6 μm, a D50 value of 16.4 μm, and a D90 value of 40.1 μm (fig. 2.2).

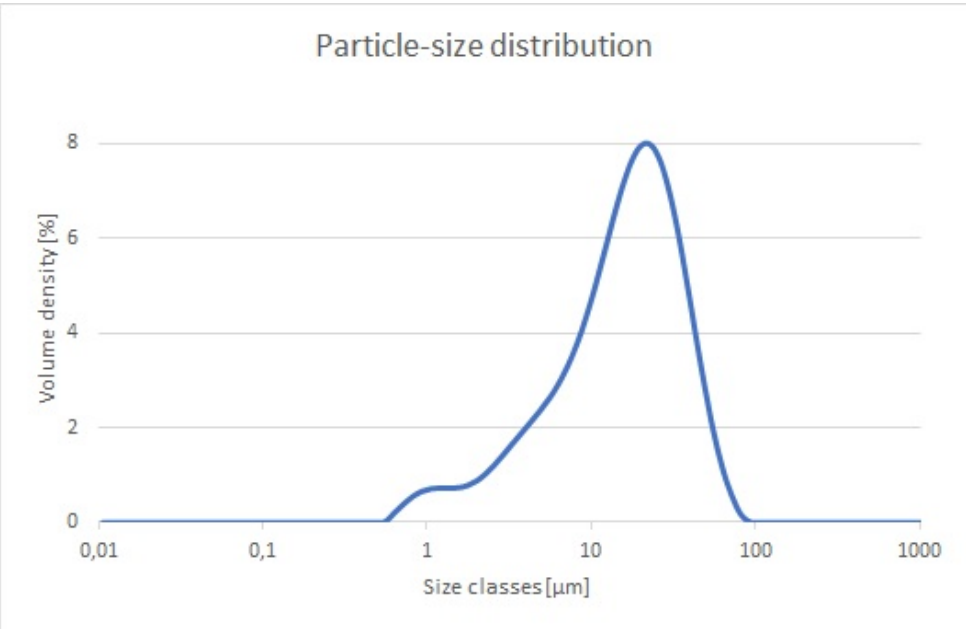

Fig. 2.2: Particle-size distribution of cement SupraCem45

2.2 Hydrated cement

In this study, to simulate the behavior of recycled concrete and accelerate the investigation of *internal sulfate attack ISA*, hydrated cement powders were used. These powders were prepared following a standardized procedure by the work of Hossam Al Daffaie in his master's thesis "Expansion phenomena during sulfate attacks" [1]. Fresh cement powders served as the starting point for this process. These cement powders were then placed into an electronic mixer, and a quantity of water equivalent to the needed *w/c ratio* was weighed before being added to the cement powder. An automatic mixing program was employed, beginning with a slow mixing phase for 60 seconds. Subsequently, the mixing briefly paused to ensure thorough blending using a spatula, followed by a 180-second duration of fast mixing under automatic control [1].

For the various cement pastes, distinct *w/c ratios* were employed: a ratio of 0.5 for *Der Blaue* and *Contragress* cement pastes and a lower ratio of 0.3 for the *Fondu* cement paste. Notably, no chemical additives, such as superplasticizers or water-reducing agents, were introduced into the mixtures. Additionally, air entrainment and the replacement of cement with pozzolanic materials were deliberately avoided to maintain simplicity and isolate the effects of *sulfate attack* on the investigated types of cement. In all tests, normal tap water was used [1].

Following the preparation of cement pastes, they were cast into steel prisms measuring 40 x 40 x 160 cm and allowed to set for one day. To prevent water evaporation during this initial curing phase, plastic sheets were placed over the mold. After one day, the prisms were de-molded and then placed in a climate chamber with controlled conditions for one month. The chamber maintained a temperature of 22 ± 2°C and a relative humidity of 63 ± 5%. To ensure optimal hydration, the prisms were positioned over a grid in a partially filled water container, elevating the relative humidity to 100%. The prisms were then dried at 60 °C for two days to make them easier to break later. This temperature was chosen since at a temperature over 60 °C destabilization of ettringite formed during the hydration process can occur, as already mentioned [1].

After the drying phase, the prisms were crushed into smaller fragments using a jaw crusher, making them suitable for the milling process. The crushed hydrated types of cement were then subjected to further grinding in a ceramic ball miller (Erich Bolling GmbH&Co) to reduce the cement into fine particles. The milling process was optimized by varying the diameter and number of ceramic balls used, striving to attain the smallest possible particle size for the hydrated types of cement. Following milling, all types of cement underwent sieving to achieve a particle size dimension below 1 mm [1].

These prepared and processed hydrated types of cement, collectively termed HF (hydrated *Fondu*), HB (hydrated *Der Blaue*), and HC (hydrated *Contragress*), were used in this study to simulate recycled types of cement. Their particle size distribution (PSD) was analyzed using a Master Sizer 3000 from Malvern Pananalytical, employing laser diffraction (fig. 2.3).

cement	Dx (10) [μm]	Dx (50) [μm]	Dx (90) [μm]
hydrate *Der Blaue*	4.70	44.90	258.00
hydrated *Contragress*	5.52	139.00	794.00
hydrated *Fondu*	2.96	36.60	145.00

Tab. 2.1: Particle size distribution of hydrated and milled cement [1]

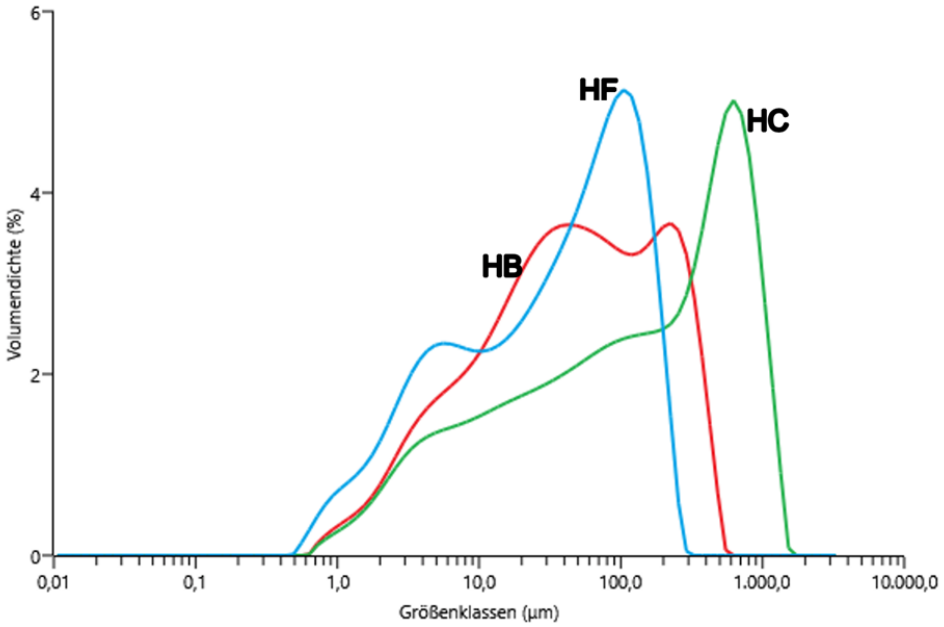

Fig. 2.3: Particle-size distribution of hydrated cement *Der Blaue*, *Fondu*, *Contragress* [1]

hydrated *Der Blaue*	
Phase	Wt. %
$C_3S + C_2S$	7.0
C_3A cubic	-
C_4AF	1.4
Ettringite	3.4
Portlandite	16.3
Hc (AFm)	1.0
Periclase	0.5
Calcite	0.5
Mc (AFm)	3.8
Am-unkn	64.4

Tab. 2.2: XRPD results of hydrated *Der Blaue* [1]

2.3 Gypsum

Fresh industrial gypsum sourced from Knauf was employed in this thesis. This gypsum was prepared by Hossam Al Daffaie [1] as follows: it was combined with water at a water-to-gypsum ratio of 0.67 and allowed to hydrate for one month. Subsequently, the resulting hydrated gypsum (HG) was subjected to drying in an oven set at 60°C for two days. Following this drying process, the HG was carefully broken into smaller fragments and sieved to ensure uniformity. The sieved HG was then categorized into two size ranges: particles smaller than 1 mm and particles within the size range of 1 to 4 mm. These segregated HG materials were instrumental in the internal contamination of the types of cement under investigation, contributing to the simulation of *sulfate attack* scenarios [1].

hydrated *Fondu*	
Phase	Wt. %
C_4AF	7.0
Hydrogarnet C_3AH_6	38.0
Gibbsite AH_3	17.0
CA	4.0
Magnesite Fe_3O_4	4.0
C2AS	2.0
Am-unkn	28.0

Tab. 2.3: XRPD results of hydrated *Fondu* [1]

hydrated *Contragress*	
Phase	Wt. %
$C_3S + C_2S$	13.0
C_4AF	6.0
Ettringite	4.0
Portlandite	14.0
Calcite	4.0
Am-unkn	59.0

Tab. 2.4: XRPD results of hydrated *Contragress* [1]

hydrated gypsum	
Phase	Wt. %
Gypsum	72.0
Dolomite	12.0
Calcite	5.0
Muscovite	3.0
Bassanite	3.0
Magnesite	2.0
Anhydrite	2.0
Quartz	1.0

Tab. 2.5: XRPD results of hydrated gypsum [1]

To gain insights into the composition of the materials and their transformation during the study, X-ray powder diffraction (XRPD) analyses were conducted. This analysis encompassed both the hydrated types of cement powders, before the addition of HG, and the HG material itself. The results of these XRPD analyses were utilized to quantify and identify the phases present in the hydrated types of cement. Notably, the analysis of the industrial hydrated gypsum revealed a composition of 72% gypsum, alongside impurities such as dolomite (12%) and calcite (5%). Furthermore, the gypsum was found to contain approximately 45% sulfate [1].

2.4 Additives

2.4.1 Calcium hydroxide

Calcium hydroxide, with the chemical formula $Ca(OH)_2$, is a compound of notable significance in various fields, including construction, agriculture, and chemistry. Commonly referred to as slaked lime, it is derived by introducing water to calcium oxide (quicklime), resulting in a chemical reaction that releases a substantial amount of heat. This process, known as hydration, transforms calcium oxide into calcium hydroxide, a white, crystalline substance that is soluble in water. In construction, it finds application in the preparation of mortars and plasters, where it contributes to setting and hardening. In agriculture, it is employed to amend soil acidity and enhance crop growth. Additionally, calcium hydroxide plays a role in various chemical processes, particularly as a reactant in laboratory experiments and industrial applications, owing to its alkaline nature and ability to influence chemical reactions[12].

In this study, calcium hydroxide was employed to accelerate the expansion process of cement samples, albeit not directly incorporated into the cement mixtures. Instead, it is strategically used within the environmental context by incorporating it into the water, used to hydrate the sample at all times.

The expedited expansion and heightened reactivity induced by the presence of calcium hydroxide in the environment lead to a more rapid response of the cementitious materials to *sulfate attack*. This aspect is instrumental in this study, enabling an in-depth exploration and evaluation of the materials' behavior under severe sulfate exposure conditions [47].

2.4.2 Magnesium oxide

Magnesium oxide (MgO), also known as magnesia, is a chemical compound with a calcination temperature of 700 °C to 1000 °C. It is produced through the calcination of magnesium carbonate or magnesium hydroxide, resulting in a fine white powder characterized by its high reactivity and exceptional thermal stability [12].

In this study, magnesium oxide is intentionally incorporated into the cement slurry to induce additional expansion. Unlike other additives that primarily serve to simulate real-world conditions, the inclusion of magnesium oxide is primarily for testing and investigative purposes. When MgO is introduced into the cement slurry, it assumes a crucial role in modifying the expansion characteristics of the samples.

The presence of magnesium oxide enhances reactivity within the cementitious matrix since it is hydrating itself faster than the clinker particles, resulting in accelerated expansion [34]. This effect is particularly valuable for the research, as it enables a thorough examination of the material responses under controlled conditions that emphasize the expansion process. By using magnesium oxide in this manner, the precision and sensitivity of the experiments are heightened, facilitating a comprehensive assessment of the materials' behavior when subjected to expansion-inducing factors.

Chapter 3

Methods

3.1 Glass ampoule-breaking test

To identify binder mixtures that expand, glass sample ampules were employed. These airtight containers are sealed due to a rubber lid and an aluminum plate, which is permanently secured to the sample container using a special clamp. The ampules used for these experiments were disposable 20 ml glass ampoules by TA Instruments originally used for a TAM Air 8-channel. In the absence of specific data on the pressure tolerance of these ampoules, a reference was made to a study that assessed the pressure sensitivity of medical ampoules. Such ampoules were shown to be able to withstand fluid pressure up to 507 kPa [42]. This comparative value served as a reliable estimate, ensuring the ampoules' capacity to withstand the forces involved in the study, despite the lack of precise pressure data.

Fig. 3.1: Glass ampoules and lids used

The mixture for filling these glass sample containers was prepared using an IKA Eurostar 40 digital (see Figure 3.19). Mixing occurs over 2 minutes at a rotation speed of approximately 500 revolutions per minute. After mixing, the cement slurry is filled directly to the brim of the sample container and immediately sealed. When sealing, care is taken to ensure that a portion of the sample overflows to guarantee that the glass is filled. The samples are then left to cure at room temperature (22°C), shielded from light, to exclude breaking by thermal effects, and monitored daily.

After 28 days, the remaining unbroken ampoules were carefully broken, and the samples were submerged in water for an additional 14 days. Before submersion, the diameter of each sample was measured. Following the 14-day immersion period, the diameters were measured once more to assess any changes or developments in the samples.

Fig. 3.2: Example for samples using the glass ampoules

3.2 Setup #1

Central to the setup is the presence of a highly rigid and confined space, which allows for minimal to no room for expansion of the cement samples. This confinement is essential for accurately measuring the pressure generated as the samples undergo hydration and expansion.

Hydration of the test samples is facilitated through a simple system. The rigid confined area is placed within a container that acts as a fluid reservoir. Above and below the sample, porous ceramic materials are strategically positioned. These ceramics serve a dual purpose: they provide an extended surface area for the sample to come into contact with water, ensuring thorough hydration, while also ensuring that the sample remains completely confined. The porous ceramic soaks up with water through small holes in the rigid confined space, placed at such a position, that the sample has no direct contact with water.

To further expedite the expansion process and simulate conditions relevant to internal sulfate attack, the entire setup is placed within an oven. The elevated temperature within the oven accelerates the chemical reactions taking place within the cement samples. Typically this reaction takes place over months or years.

Within this setup, the expansion of the cement samples is primarily constrained in the vertical direction. Therefore, to measure the pressure accurately, a load cell is integrated into the system. This load cell needs to be calibrated to record the force exerted by the expanding samples, allowing for precise measurement and analysis of the pressure generated during the expansion process.

The first schematic of the setup is shown in figure 3.3.

To create a rigid confined space for housing the test sample, a steel tube with an outer diameter of 5 cm and an inner diameter of 3 cm was custom-fabricated (see figure 3.7). This steel tube is constructed from stainless steel S235 to prevent rusting. At one end of the tube, a threaded

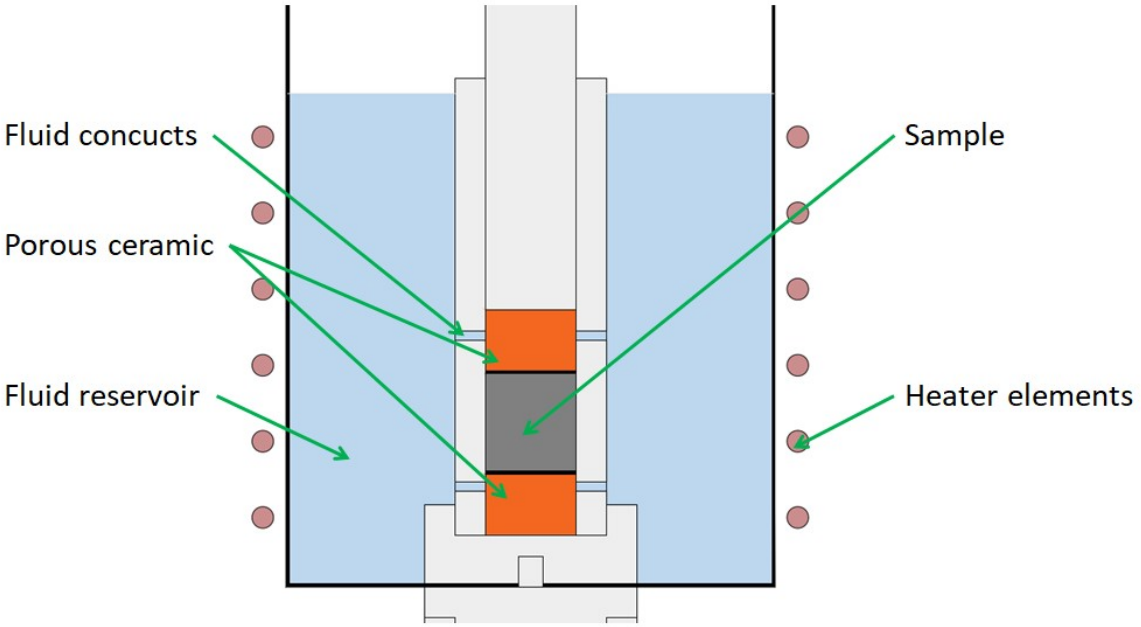

Fig. 3.3: Initial diagram of the setup

cap is affixed, allowing for secure closure (figure 3.8). The tube is equipped with six small holes, each measuring 1.5 mm in diameter, with three located within the first 2 cm of the tube and three positioned between 5 and 7 cm. These holes serve as conduits for irrigating the porous ceramic material surrounding and encompassing the test sample. See figure 3.7b.

The concept behind this design is to ensure that the porous ceramic material, both above and below the sample, has a consistent height of 2 cm, while the sample itself occupies a central height of 3 cm. The small holes facilitate the controlled hydration of the porous ceramic. For the ceramic Poroton-Mz NF-2,0 from Wienerberger was cut and used (figure 3.11).

To seal the top of the tube and provide a platform for a load cell, a piston with a 3 cm diameter, made from the same material as the tube, is employed(figure 3.10). This piston, with a length of just over 60 cm, incorporates a centering pin at its upper end to facilitate the precise alignment of the load cell. The steel tube, cap, and piston assembly are connected to a base element (figure 3.9) via threaded connections. Between the cap and the base element, a metal container is secured and sealed with an O-ring. This container functions as a water reservoir (figure 3.12, ensuring continuous hydration of the test sample. The entire setup is placed within an oven (RHODE TE 10 Q 2006, load 1,8 kW. supply 8 A, electricity 1N/PEAC 230V, maximum operating temperature 1320°C), which is insulated on five sides and equipped with temperature control capabilities. See figure 3.13. This oven should be able to maintain a specific temperature over an extended period.

In the first experimental campaign, a steel frame is utilized. This frame consists of two vertical UPN120 S235 profiles, each 1.40 meters in length, connected at the top and bottom to two UPN100 S235 profiles, each 55 cm long. All structural components are interconnected using bolted connections. See figure 3.6.

The lower part of the setup rests on a steel plate made of S235 construction steel, measuring 15 cm by 15 cm and with a thickness of 2 cm. In the upper part, a similar steel plate with the same properties and dimensions is affixed. This upper plate features two M30 nuts welded to it,

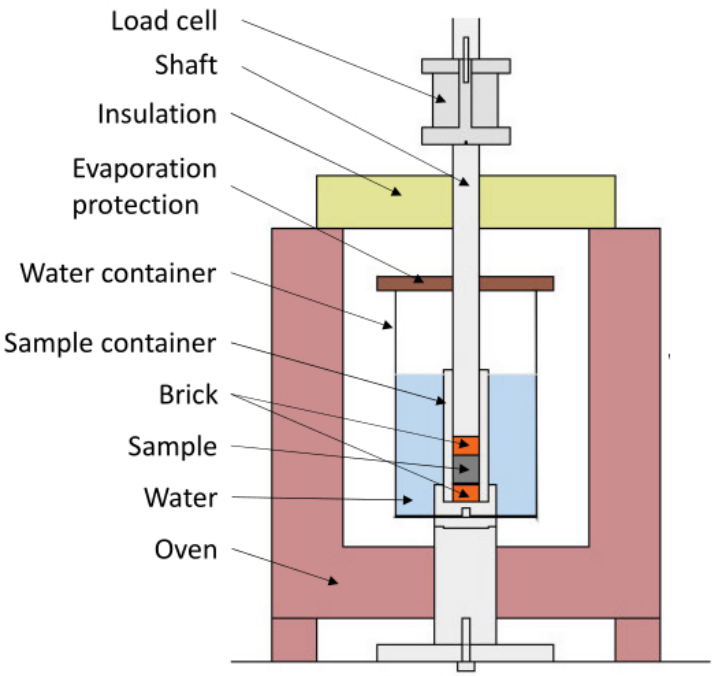

Fig. 3.4: Scheme of the first setup

which guide a non-corrosive stainless steel threaded rod (M30 with a 1.5 mm thread pitch). This threaded rod allows for adjustment of preloading once the sample is positioned within the setup. Such preloading is essential for ensuring proper contact with the sample.

The load cell employed in the setup is identified as the CN500 model from Hottinger Brüel & Kjær, featuring thermal correction capabilities. Temperature measurements are obtained from two separate sources. Thermocouples of Type K, also provided by HBM, are used. One thermocouple is placed between the water reservoir and the oven, monitoring the oven temperature as a reference for the oven built-in temperature sensor. The second thermocouple is immersed in the water reservoir, measuring the water temperature.

To monitor any potential deformation of the entire setup, two displacement sensors are installed, initially positioned at the left and right ends of the frame. These sensors, extended with multi-layered plate rods, span the entire distance from the upper to the lower support beams. These displacement sensors, supplied by HBM and designated as Model WA-T with a capacity of up to 100 mm, facilitate the measurement of any expansion or contraction in the frame.

3.3 Problems with setup #1

The setup #1 for this study presented several challenges. Firstly, setting up the sample proved to be cumbersome and time-consuming due to the fine-threaded adjustment using a threaded rod. Ensuring a secure attachment of the sample and applying a preload took a substantial amount of time. Additionally, the fine-threaded rod posed problems as even the slightest turns generated high forces that were undesirable and could distort the results.

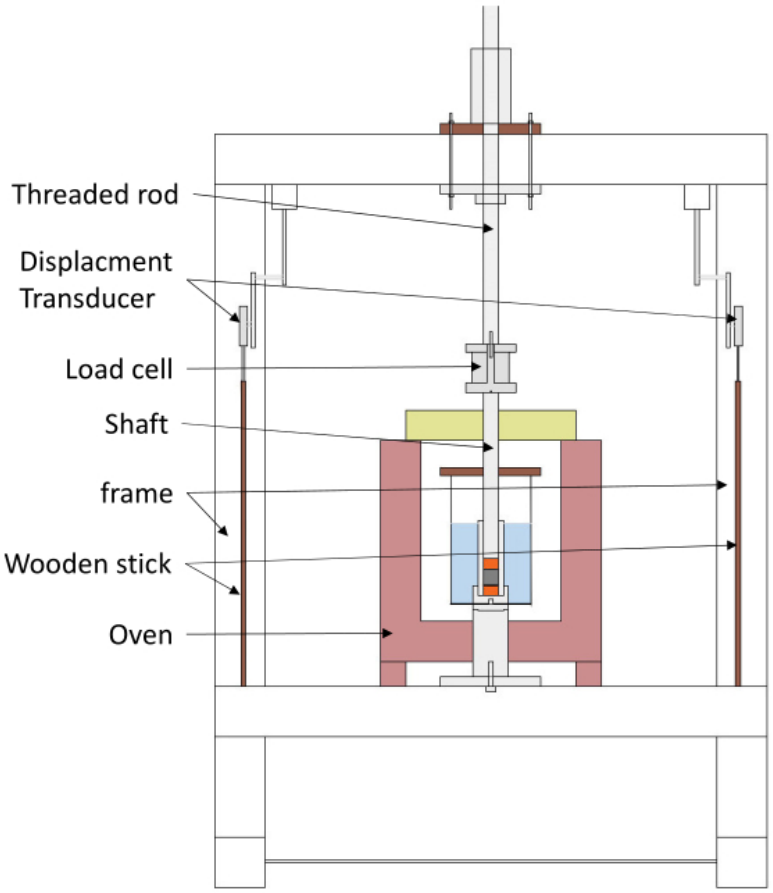

Fig. 3.5: Scheme of the first setup with steel frame

Another significant issue arose in the form of compliance of the frame, even under minimal forces of approximately 0.2 kN. These deformations exceeded 0.2 mm, and this measurement did not even consider the deflection of the horizontal UPN beams, which were initially considered negligible given the expected forces of up to 10 kN in these experiments. With a sample height of 3 cm, a deformation of 0.2 mm was already excessive, leading to a distortion of the results. To eliminate the possibility of deformation in the wooden elements used as extensions for the displacement sensors, the system for deformation measurement was altered. One displacement sensor was placed directly beneath the load-bearing horizontal UPN beams to measure deflection, while the other remained on the side to capture changes in the vertical elements of the frame. However, even after excluding the wooden rods, similar deformations persisted, rendering this frame unsuitable for the experiments in its current configuration.

Another challenge emerged during the heating of the sample to accelerate the process. Thermal-induced deformations, particularly in the piston and other steel components inside the oven, significantly affected the confinement, overshadowing the desired results. To mitigate this issue,

Fig. 3.6: Steel frame used at the beginning

(a) front view **(b)** Fluid conduits

Fig. 3.7: Sample container

Fig. 3.8: Bottom cap of main setup

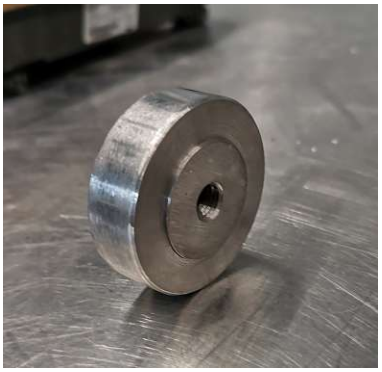

Fig. 3.9: Bottom connector of main setup

Fig. 3.10: Piston for sealing of the sample

Fig. 3.11: Porous ceramic used: brick

(a) Front view

(b) Top view

Fig. 3.12: Water reservoir

(a) Front view

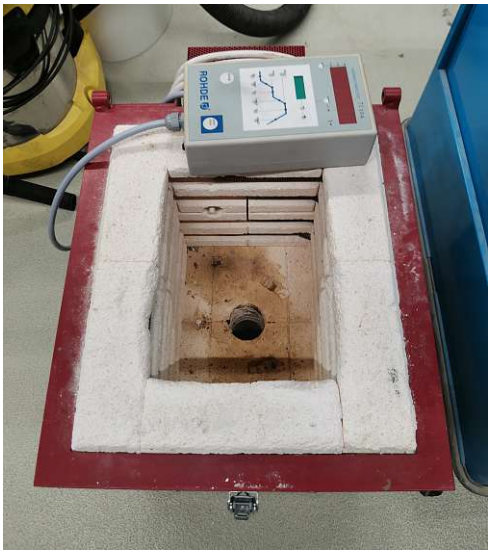

(b) Top view

Fig. 3.13: Oven for controlling temperature - ROHDE TE 10 Q 2006

Fig. 3.14: setup #1

precise temperature control was essential, requiring preheating of all setup elements, including the water, and maintaining an accurate temperature. However, the disassembly and reassembly of the setup for sample loading led to rapid cooling of the steel components, a challenge that was difficult to prevent. Consequently, one had to wait for the setup to return to the required temperature before commencing measurements, which took approximately one minute. It is worth noting that the primary goal was to measure the sample during the curing and post-curing stages, not when it was still in a liquid state.

A further complication related to temperature control stemmed from the inability of the used oven to maintain an exact temperature. Over extended periods, temperature fluctuations within a range of plus or minus 0.5°C were observed. These fluctuations induced thermal expansion in the steel elements, resulting in noticeable fluctuations in the measured force readings.

3.4 Setup #2

To address the primary issue of frame deformation, a significant modification was made to the frame of the setup by integrating the core of the setup into a ZWICK Z250 (figure 3.16). This ZWICK setup has much lower compliance, and offers precise position adjustments, greatly enhancing its overall usability. Consequently, the load cell was also changed, with the already integrated load cell in the ZWICK now being utilized. The displacement sensors were no longer

necessary as the ZWICK inherently performs positional measurements. To compensate for any potential misalignment in the system, a spherical joint was employed. Both the oven and the temperature measurement devices remained consistent.

Before conducting the experiments with the setup, a compliance test, i.e. without a sample, was performed in the empty state of the setup using the ZWICK system, as illustrated in figure 3.15. The results of this test can be considered during the evaluation of the experimental outcomes, ensuring that any non-negligible deviations could be appropriately accounted for. This finalized setup offered improved stability, precise measurements, and reliable control over potential sources of error, enhancing the accuracy.

To establish an approximate relationship between force and deformation in the setup #2, a linear trendline was created. This trendline reveals that, with this setup, a force of 1000 N induces a deformation of 0.02 mm. Consequently, this setup allows for a sample deformation of 20 micrometers per kilonewton of force (see equation 3.1, which is not considered in the force generation. This deformation corresponds to 0.00066% of the sample height (at 3 cm), thus falling within the negligible range, even with forces as high as 10 kN. Given that maximum forces in this range were anticipated, this setup is deemed sufficient for the experiment requirements.

$$F_{exp} = 51.788 \frac{N}{\mu m} * u_{exp} \tag{3.1}$$

F_{exp} [N] = vertical force on setup

u_{exp} [μm] = vertical absolut deformation

Fig. 3.15: Compliance test with ZWICK setup; $F_{exp} = 51.788 \frac{N}{\mu m} * u_{exp}$

Fig. 3.16: ZWICK Z250

Fig. 3.17: setup #2

3.5 Temperature control

The control of temperature within the experimental setup is a important factor, especially in the context of accelerating the sulfate attack process to reduce the duration of experiments. To achieve this, an oven is utilized within which a part of the setup resides during the experiment. This oven measures the temperature T_{AO} at its inner lower edge using a built-in sensor and accordingly regulates its heating elements. Additionally, the temperature of the water in the water reservoir T_W is recorded. Due to the incomplete filling of the water reservoir, an air space forms between the evaporation protection and the water surface, resulting in an air temperature T_{AR} in this area.

All these temperatures – T_{AO}, T_W, and T_{AR} – should ideally stabilize before the commencement of the experiments. This stabilization ensures that temperature variations do not influence the experimental results. The room temperature T_R also plays a significant role since parts of the setup are located outside the oven and are thus exposed to room conditions. The thermal insulation of the oven, supplemented by additional insulation serving as a lid, separates the room temperature from the oven temperature.

In the steel components of the setup, transitional areas arise that do not clearly align with any of these specific temperatures. To simplify this factor, a temperature jump is assumed in the middle of the separating components. Figure 3.18 illustrates this setup, showing that the sample, the porous ceramic, and a total of 9 cm of steel elements are exposed to the water temperature T_W. An additional 2.7 cm of steel length is exposed to the air temperature T_{AR} in the reservoir, 12.4 cm to the oven air temperature T_{AO}, and the remainder to the room temperature T_R.

For the experiment to yield meaningful results, all temperatures within the oven and the room temperature must remain constant. This constancy is crucial to exclude thermally induced expansions, allowing focus on the expansion behavior in a confined space by the sample. It is important to note that air reacts more quickly to temperature changes than water, which can lead to a delayed correlation between temperature changes, as the temperature is measured in the water reservoir, and expansion behavior if the temperature profile is not stable.

Furthermore, if temperatures T_{AO}, T_W, and T_{AR} differ from each other this leads to additional temperature differences within the components of the setup.

The stainless steel used in the setup has a thermal expansion coefficient of $\alpha = 17 * 10^{-6} \frac{1}{K}$ in the temperature range of 20°C to 300°C. With equation 3.2 [13], the change in length and consequently the variation in confinement can be calculated. However, as the steel does not have space to expand freely, a significant portion of this expansion is restricted and is thus recorded as pressure. To calculate this pressure equation 3.3 [13] is used with $E = 210$ GPa at up to 100°C.

$$\Delta l = \alpha * l_0 * \Delta T \tag{3.2}$$

$$\sigma = E * \alpha * \Delta T \tag{3.3}$$

3.6 Procedure of setting up the sample

The sample setup procedure followed a structured sequence as outlined below:

1. Preheat the setup to 50°C.
2. Preheat the water to 50°C.
3. Soak the two brick elements in water.

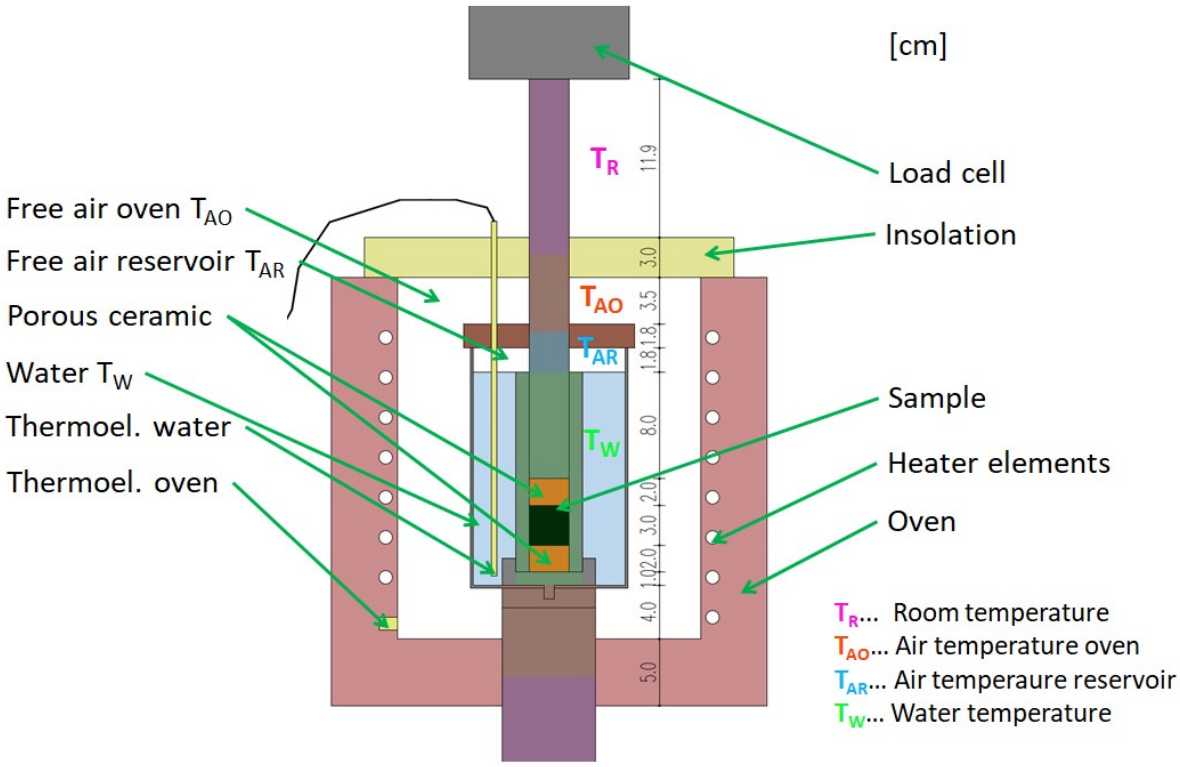

Fig. 3.18: Temperature scheme of setup

4. Prepare the components for the sample.
5. Mix the sample.
6. Fill the sample into a syringe.
7. Remove the setup from its position.
8. Place the lower brick.
9. Position a filter paper.
10. Inject the sample using the syringe.
11. Eliminate any air bubbles with a thin rod.
12. Hand compact the sample with slight pressure using the piston.
13. Place another filter paper.
14. Position the upper brick.
15. Set the piston in place.
16. Reassemble the setup promptly.
17. Apply a preload of 100N.

18. Release the preload.
19. Apply the preload of 100N again.
20. Check the water temperature and adjust if necessary to 50°C.
21. Fill the water reservoir.
22. Seal the water reservoir.
23. Place insulation on top of the oven.
24. Start the measurement at least 1 minute after filling the water.
25. Let the test run for several days.

As previously mentioned, preheating the water and the entire setup is crucial to minimize temperature-induced deformations. It is essential to wait briefly before initiating the measurement to allow the disassembled elements to reach the desired temperature again. One minute has proven to be sufficient when the sample is inserted quickly. The brick elements are saturated with water to prevent them from drawing moisture away from the sample, which is possible due to their high porosity. The sample consists of at least 100 grams of dry material to ensure adequate mixing. The mixture is prepared using an IKA Eurostar 40 digital (see figure 3.19). Mixing occurs over 2 minutes at a rotation speed of approximately 500 revolutions per minute. After mixing, a syringe is filled with 22 milliliters, equivalent to a sample height of 3 cm given a diameter of 3 cm. Filter paper is placed in between the ceramic material and the sample to prevent the leaching of cement particles. The preload of 200N is applied twice since, during the first application, the force is rapidly lost within seconds. The ZWICK is configured to maintain the position after achieving the preload. However, likely due to adjustments of the setup and reorganization of the cement mixture under the applied force, the preload is lost, necessitating its reapplication. Additionally, the water reservoir is sealed to minimize water evaporation over the running time of the experiment.

The experiments conducted in this study involve the measurement of a force, which comprises two essential components that need consideration: the pre-existing force that must be subtracted, and the weight of the piston that exerts an additional force on the sample. The weight of the stamp, 1633 grams or equivalently 16 Newtons, should be factored into the final result. Thus, the calculation can be summarized as follows: the result obtained from the experiments minus the pre-existing force plus the force exerted by the weight of the stamp (see equation 3.4).

$$F_{measured} - F_{preload} + F_{piston} = F_{SA} \tag{3.4}$$

To convert this force into stress as needed, it needs to be divided by the constant surface area of the sample, which remains the same for all experiments (see equation 3.5). This consistency is maintained due to the circular shape of the surface, which possesses a diameter of 30 mm.

$$\frac{F_{SA}}{S_{sample}} = \sigma_{SA} \tag{3.5}$$

F_{SA} = force induced by sulfate attack under confined area

S_{sample} = surface area of the sample in the direction of load cell

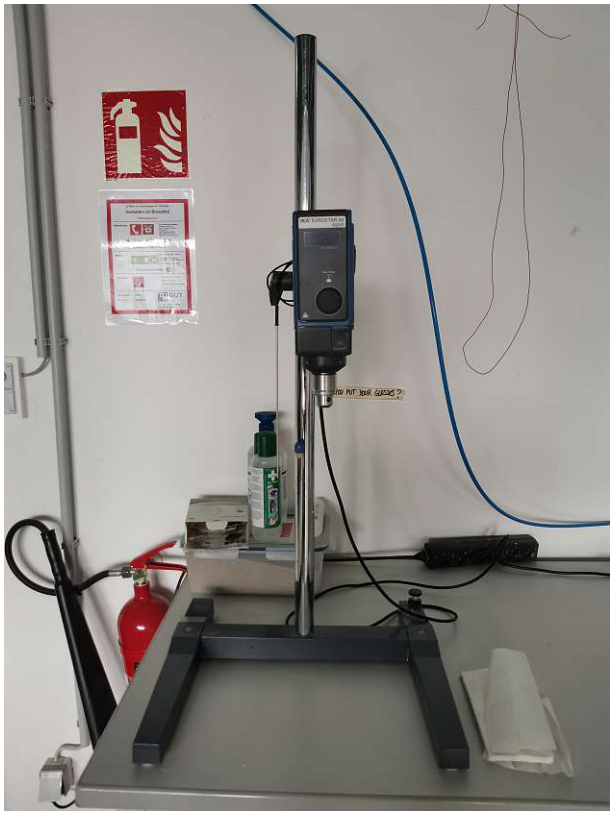

Fig. 3.19: IKA Eurostar 40 digital used for mixing the samples

Chapter 4

Results and discussion

4.1 Results of glass ampoules breaking experiment

The glass ampoule-breaking experiments involved the preparation of various mixtures to investigate their ability to generate sufficient pressure to break the glass containers. These mixtures included:

1. Cement hydrated *Der Blaue* and 5% Magnesium oxide
2. Cement hydrated *Der Blaue* and 10% Magnesium oxide
3. Cement hydrated *Der Blaue* and 20% Magnesium oxide
4. 85% hydrated cement *Der Blaue*, 15% hydrated cement *Fondu* and 50% of cement hydrated gypsum
5. Cement *SupraCem45* and 100% of cement hydrated gypsum
6. Cement *SupraCem45*, 100% of cement hydrated gypsum and 5% of binder magnesium oxide
7. Hydrated cement *Fondu* and 100% of cement hydrated gypsum

Each mixture was prepared using at least 100 g of binder and followed the procedures outlined in section 3.1.

Mixture	HB [g]	HF [g]	SC45 [g]	Gypsum [g]	MgO [g]	w/b	break point [d]
1	100	-	-	-	5	0.45	-
2	100	-	-	-	10	0.45	-
3	100	-	-	-	20	0.45	20
4	85	15	-	50	-	0.41	-
5	-	-	50	50	-	0.50	14
6	-	-	50	50	5	0.50	14
7	-	50	-	50	-	0.45	-

Tab. 4.1: Mixtures for glass ampoules breaking test

Among these mixtures, only three exhibited the ability to break the glass containers. The first notable combination were both SupraCem45 mixtures, which achieved glass breakage after 14 days.

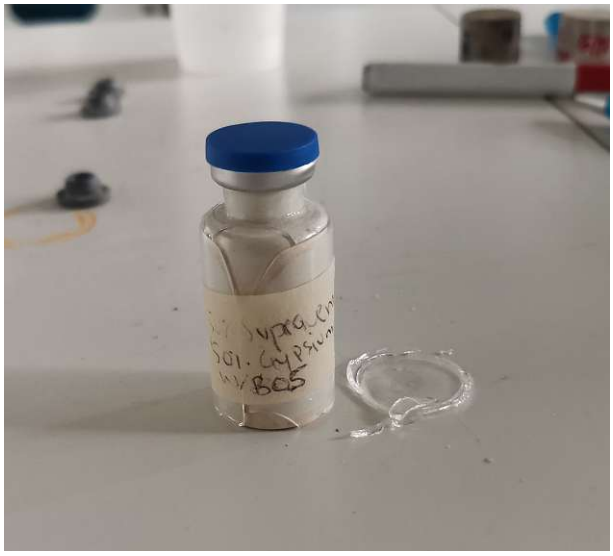

Fig. 4.1: Broken glass sample *SupraCem45* and Gypsum

The third mixture, cement hydrated Der Blaue + 20% magnesium oxide, exhibited glass breakage after 20 days. The inclusion of 20% magnesium oxide likely contributed to delayed expansion and pressure generation.

Interestingly, after immersing the broken samples in water for an additional 14 days, no changes in sample diameter were detected. This indicates that the initial pressure generated by these mixtures was sufficient to break the glass, but there was no significant expansion or continued pressure development during the subsequent immersion period.

Overall, these findings highlight the varying capabilities of different cement mixtures in terms of force generation and expansion potential, with SupraCem45 showing the fastest results in breaking the glass containers. However, it is essential to consider the practical implications and limitations of these results when applying these cement mixtures in other study applications.

4.2 Results of expansion in a confined environment experiment

The study involved multiple experiments using the setup #1; however, the results obtained from these initial trials lacked significance due to a multitude of problems, as discussed in section 3.3. Consequently, this section focuses solely on the results obtained from the setup #2, which is presented and discussed here.

For these experiments, various samples were prepared, including:

- *SupraCem45*, hydrated gypsum and magnesium oxide
- *Der Blaue* and hydrated gypsum
- Hydrated *Der Blaue*, hydrated *Fondu* and hydrated gypsum

All experiments were conducted as described in section 3.6, with variations in the duration of each experiment. The primary objective was to assess the functionality of the setup and gain insights into the expected force ranges generated by these experiments. The experimental outcomes from the setup #2 are analyzed and discussed in detail below.

4.2.1 Test 2.5 *SupraCem45*, hydrated gypsum and magnesium oxide

Test 2.5 marked the initiation of experiments using the finalized setup, which included a mixture of *SupraCem45*, hydrated gypsum, and magnesium oxide. This specific composition can be referenced in table 4.2. *SupraCem45*, renowned for its swift reactivity, in combination with gypsum, facilitates the rapid formation of ettringite. The introduction of magnesium oxide was essential to further stimulate expansive reactions. This choice of a fast-reacting mixture aimed to achieve a two-fold goal: to assess the functionality of the experimental setup and to categorize the forces generated specifically by this mixture. Since we had trouble with stabilizing the setup, still not an optimized procedure of setting up the sample, and some other problems we decided to end the total runtime of the experiment after only 68 hours and move on to the next experiments. Therefore a higher pressure might have been measured, if we had let it run for at least 14 days as shown in the preliminary tests with the glass ampoules.

Test 2.5	
SupraCem45	50 g
hyd. Gypsum	50 g
water in sample	51 ml
water / binder	0.51
magnesium oxide	5 g
water in reservoir	1.2 L
calcium hydroxide in reservoir	15 g
calcium hydroxide solution	1.25 %
sample height	3 cm
preload left after 5 minutes	118 N

Tab. 4.2: Composition Test 2.5 *SupraCem45*

During the test, an adjustment in the oven temperature setting was necessitated due to preliminary complications arising from excessively high temperatures. These elevated temperatures led to undesired thermal-induced deformations within the setup. The adjustment sought to mitigate these temperature-related issues.

An analysis of these concurrent graphs of temperature and measured force (figure 4.2) reveals a distinctive surge in temperature during the initial 10 hours of the test. This temperature spike substantially influenced the recorded forces within this timeframe. However, as the temperature stabilized beyond the tenth hour, the measured forces became primarily attributed to the formation of secondary ettringite in the sample.

At approximately the twentieth hour, the oven experienced irregularities, leading to a slight increase in temperature. This resulted in an immediate and corresponding increase in the measured forces. Subsequently, around the 22.5-hour mark, the oven temperature was deliberately reduced to confirm suspicions regarding thermal-induced pressures. Furthermore, the initial temperature setting of the oven proved to be too high. The novel setup was designed to minimize heat losses, subsequently reducing the temperature difference between the oven and water. As depicted in the graph, the force development responded rapidly to the lower temperature, resulting in a significant decrease.

Notably, even as the temperature continued to decrease, an increase in force was observed after the thirtieth hour. By the fortieth hour, the temperature had stabilized, leading to a more consistent force development. Figures 4.3 and 4.4 serve as detailed representations of the two specific segments in which temperature was stabilized. This allowed for a focused examination of the expansive behaviors within these temporal windows.

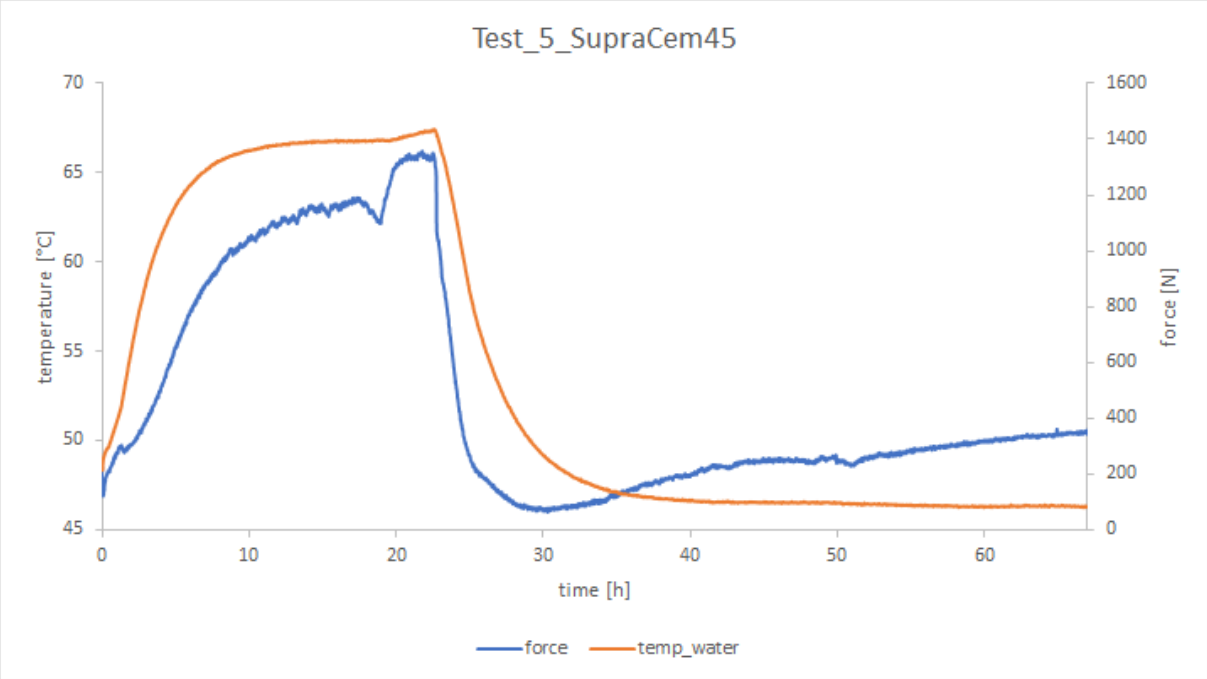

Fig. 4.2: Force and temperature development test 2.5

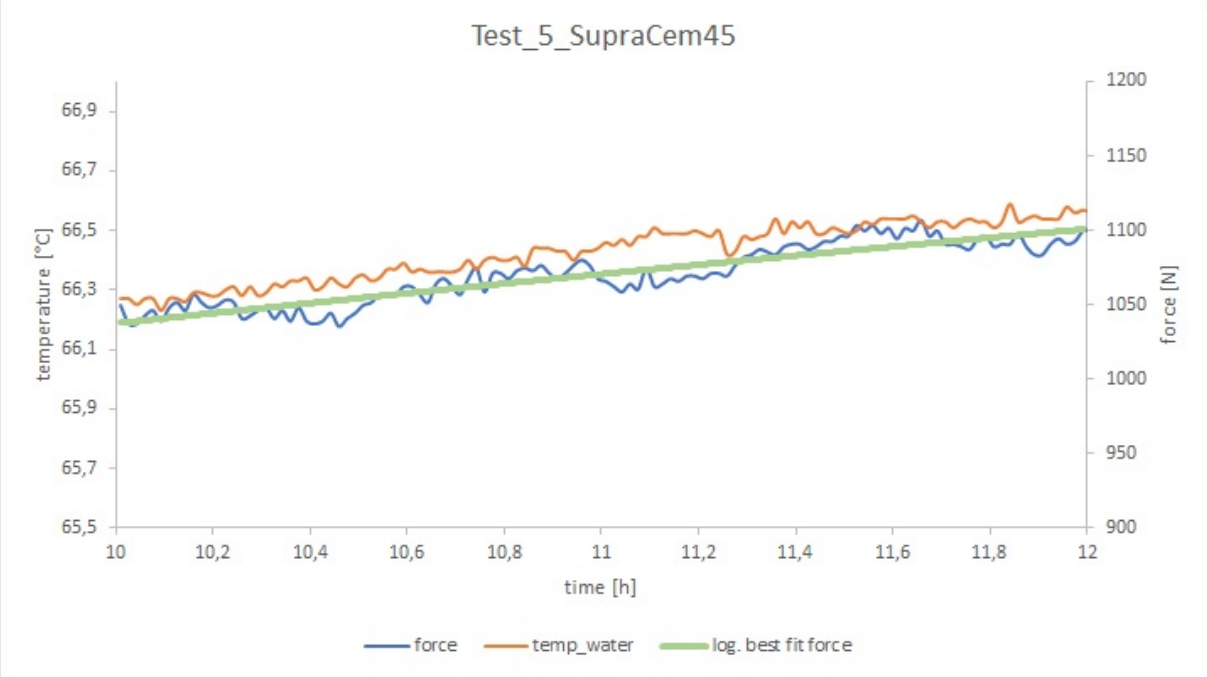

Fig. 4.3: Sequence 10h – 12h test 2.5

In this experiment, it is important to note that the maximum measured force is not particularly informative due to the loss of confinement due to the thermally induced expansion of the setup. Instead, the primary focus is placed on the evolving force profile over time.

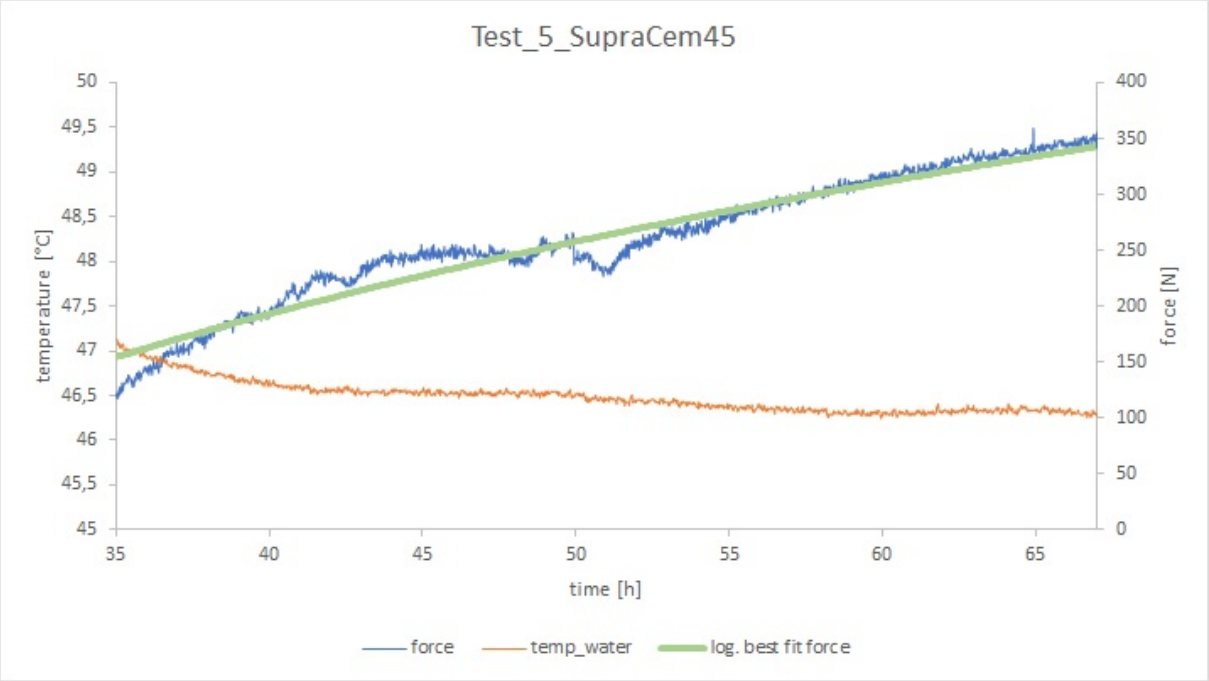

Fig. 4.4: Sequence 35h – 68h test 2.5

4.2.2 Test 2.6 *Der Blaue* and hydrated gypsum

In Test 2.6, we examined a mixture composed of fresh *Der Blaue* cement and hydrated gypsum. This combination is of particular interest as it could mimic conditions that one might encounter when working with recycled concrete, offering results that can be applied to practical scenarios. The exact composition of this mixture can be found in table 4.3. The experiment extended for 160 hours, which is approximately one week. In contrast to earlier tests, the oven temperature was correctly set from the beginning. However, it took ten hours for the water temperature to stabilize, leading to a gradual decrease of approximately 1.3°C from its initial temperature.

Test 2.6	
Der Blaue fresh	50 g
hyd. Gypsum	50 g
water in sample	50 ml
water / binder	0.50
water in reservoir	1.2 L
calcium hydroxide in reservoir	18 g
calcium hydroxide solution	1.50 %
sample height	3 cm
preaload left after 5 minutes	30 N

Tab. 4.3: Composition Test 2.6 *Der Blaue*

Despite these initial challenges, a trend in force development can be seen. The preload, just a few minutes after the test initiation, had declined to 40 N. By the twentieth hour, the force had surged to 140 N. This rapid rise in force suggests an intense early-stage reaction between the cement and gypsum. As the experiment progressed, the rate of force increase began to taper

off. Temperature fluctuations changed the confinement and this shows through the oscillating behavior of the force measurement over time (figure 4.5). However, by employing a trendline to the measured data, it became evident that there was a sustained upward force progression throughout the experiment duration, as depicted in figure 4.6.

The oscillating behavior observed in the experiment reveals that the temperature fluctuates within a range of approximately 0.3°C, while the measured force varies within a scope of about 70 N. Applying equations 3.2 and 3.3 from chapter 3, section 3.5, the theoretical expansion of the steel components is estimated at 1.2 μm under unrestricted conditions. Correspondingly, this expansion would generate a pressure of 63 kPa, equivalent to a force of 178 N when calculated over the sample surface area, assuming complete restriction of the expansion. By comparing the measured force with the calculated value, it is evident that a combined effect of expansion and its restriction is occurring. This results in an alteration of the confinement, approximately in the order of 0.8 μm.

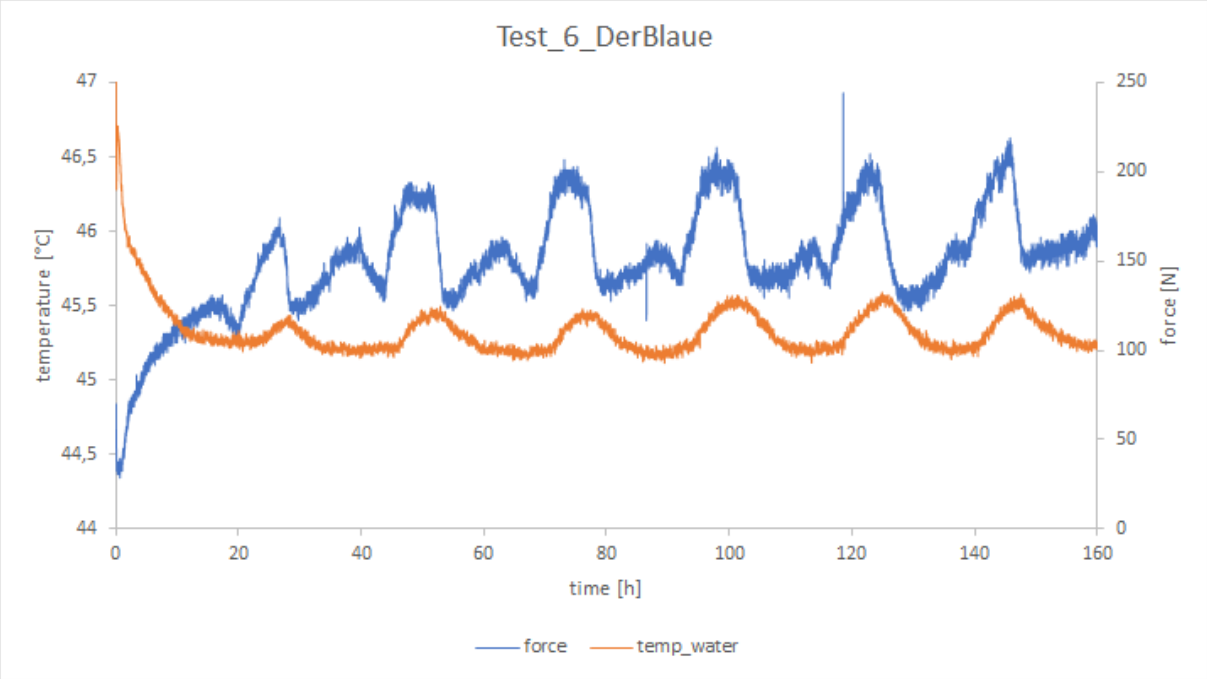

Fig. 4.5: Force and temperature development test 2.6

At the end of the experiment, the recorded force value was 156 N after using the equation 3.4. This translates to a stress of 220 kPa (see equation 3.5). However, it is worth noting that the maximum measured force may not be fully indicative due to the influence of thermally induced forces on the setup and a runtime of only one week.

4.2.3 Test 2.7 Hydrated *Der Blaue*, hydrated *Fondu* and hydrated gypsum

For Test 2.7, we employed a cement mixture composed entirely of hydrated materials. This included 85% hydrated *Der Blaue*, 15% hydrated *Fondu*, and hydrated gypsum, with a test duration of approximately 355 hours. This composition was chosen based on previous experiments where a higher volume expansion was observed. The intention was to induce an equally high compressive stress when the volume was constrained. The precise composition can be found in table 4.4. Due to recurring issues with the furnace, a temperature increase of approximately 1.8 °C was recorded in the reservoir water. Subsequently, the temperature steadily decreased, almost

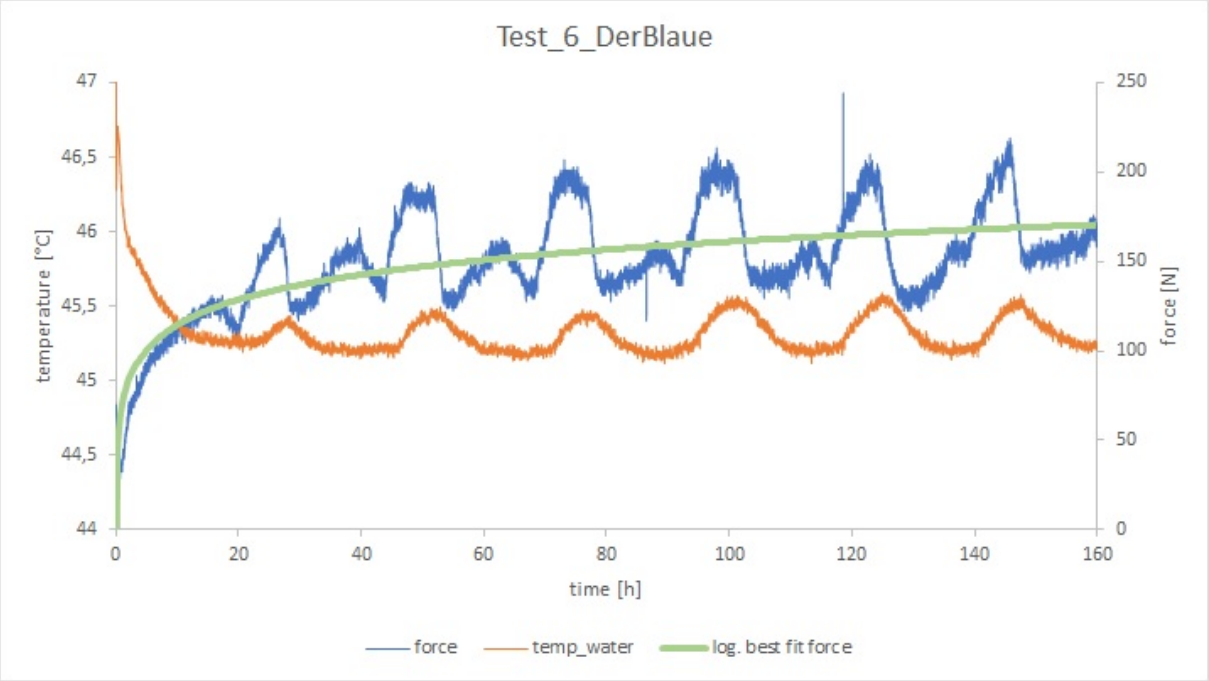

Fig. 4.6: Force development – Trendline test 2.6

reaching the initial value. Fluctuations within the range of +/-0.3 °C occurred consistently throughout the entire test duration, mirroring patterns observed in preceding experiments.

Test 2.7	
hyd. *Der Blaue*	85 g
hyd. *Fondu*	15 g
hyd. Gypsum	50 g
water in sample	52.5 ml
water / binder	0.35
water in reservoir	1.2 L
calcium hydroxide in reservoir	15 g
calcium hydroxide solution	1.25 %
sample height	3 cm
preload left after 5 minutes	60 N

Tab. 4.4: Composition Test 2.7 HB and HF

Examining the force evolution, the initial 13 hours witnessed a substantial increase, primarily attributed to thermally induced forces from the steel elements. Even after reaching its zenith at the thirteenth hour of temperature, the force continued to rise, ultimately reaching a value of 982 N after the entire test duration. Subtracting the remaining pre-existing force after two minutes, amounting to 46 N, yields a final force of 936 N. The simultaneous examination of the force evolution and temperature reveals a notable divergence after the thirteenth hour. The decreasing temperature of 0.004 Kelvin per hour correspondingly lowers the thermally induced expansion from the steel elements, and in the absence of sample expansion, the force should decline. However, the persistent force increase of around 1 Newton per hour suggests that it would be substantially higher if the temperature did not decrease. While it is reasonable to

assume that the distortion of results due to the initial temperature increase is compensated by the constant decline until the end of the experiment, certainty in this regard is challenging. In figure 4.8, the force evolution is further illustrated with a trendline depicting the logarithmic rise in force. Trimming the initial 20 hours from the graph (see figure 4.9) accentuates the logarithmic progression, resulting in compressive stress that may be primarily induced by *sulfate attack* of 1.39 MPa. Since we have no exact data on the confinement of the setup during the experiment, there is no way to be certain, that this pressure can be attributed completely to the process of *sulfate attack*.

Fig. 4.7: Temperature development test 2.7

4.3 Problems and limitations of the significance of the results

The significance of the results obtained in this study is affected by several problems and limitations associated with the experimental setup. As discussed in chapter 3 section 3.3, although some of these issues were addressed, not all of them could be completely resolved. A prominent challenge is the fluctuation in temperature, which is notably evident in the test results. Temperature variations are induced both by the oven characteristics and the system high confinement. Even small temperature fluctuations on the order of tenths of a degree lead to substantial variations in the measured force compared to the absolute values.

The complex arrangement of the system, partly within the oven and partly outside, results in the temperature of individual components being influenced by both the oven and the surrounding room temperature conditions as already mentioned in chapter 3 section 3.5. The part of the system submerged in water is more stable in terms of temperature due to the heat capacity of water. However, the portion exposed to the oven airspace experiences highly dramatic temperature sensitivity. The phenomenon described is particularly evident in figure 4.10 from Test 2.6, where the relationship between force and temperature becomes strikingly apparent. In this case, there is a noticeable discrepancy between the force increase and the temperature

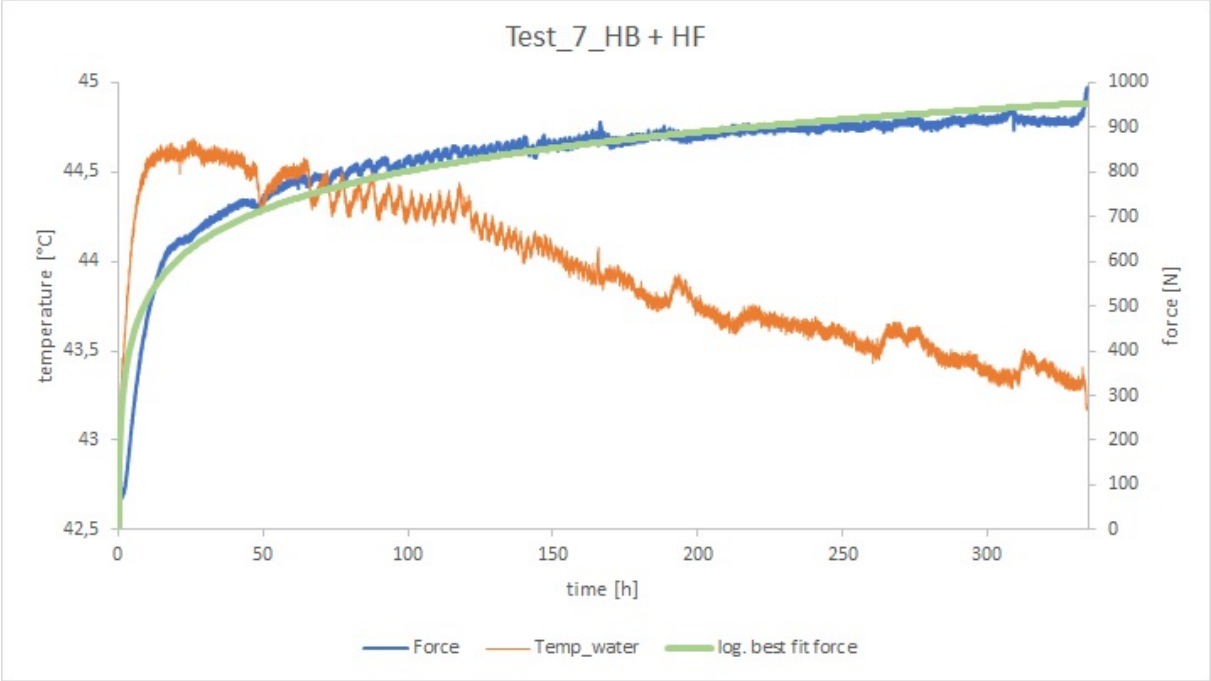

Fig. 4.8: Temperature development test 2.7

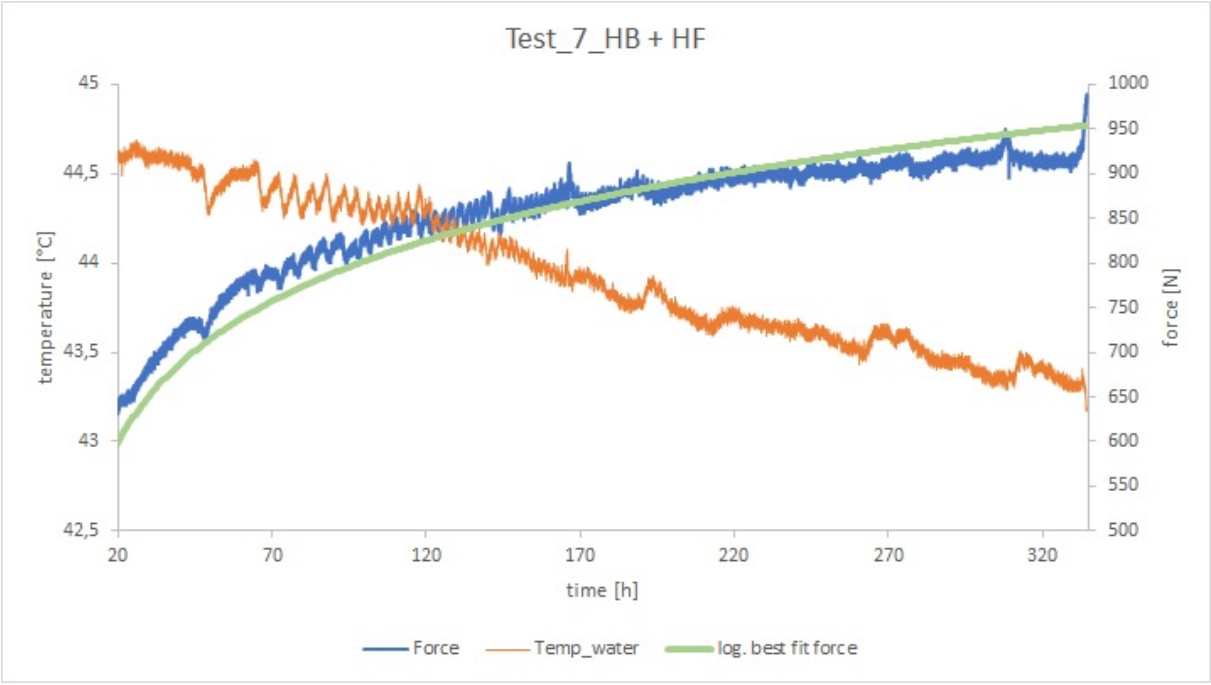

Fig. 4.9: Temperature development test 2.7

rise, deviating from what one would intuitively expect based on basic physics. However, this behavior can be attributed to the structure of the system. The explanation lies in the piston position within the oven, specifically in the airspace of the oven. This positioning results in a rapid response of the piston to any temperature changes occurring within this region. When the temperature inside the oven shifts, the piston reacts promptly by expanding. Although thermally

induced, this expansion generates a force that registers on the measurements. Essentially, it is an indirect result of the piston immediate response to temperature fluctuations. The area outside the oven, situated above the insulation, introduces another layer of complexity to the system. In this region, the piston is significantly affected by the ambient room temperature. This dynamic environment results in temperature fluctuations driven by two key factors. First, heat conduction from the oven interior causes temperature variations in the piston, making it responsive to changes in the oven temperature settings. Second, the piston temperature is also subjected to fluctuations in the room temperature. Predicting a clear and consistent temperature profile in this setting is a challenging task, especially under the prevailing experimental conditions. This disparity creates a continuously changing temperature profile along the length of the piston. This complex temperature profile, in conjunction with the system response to temperature changes, introduces significant fluctuations in force measurements, making it challenging to quantify.

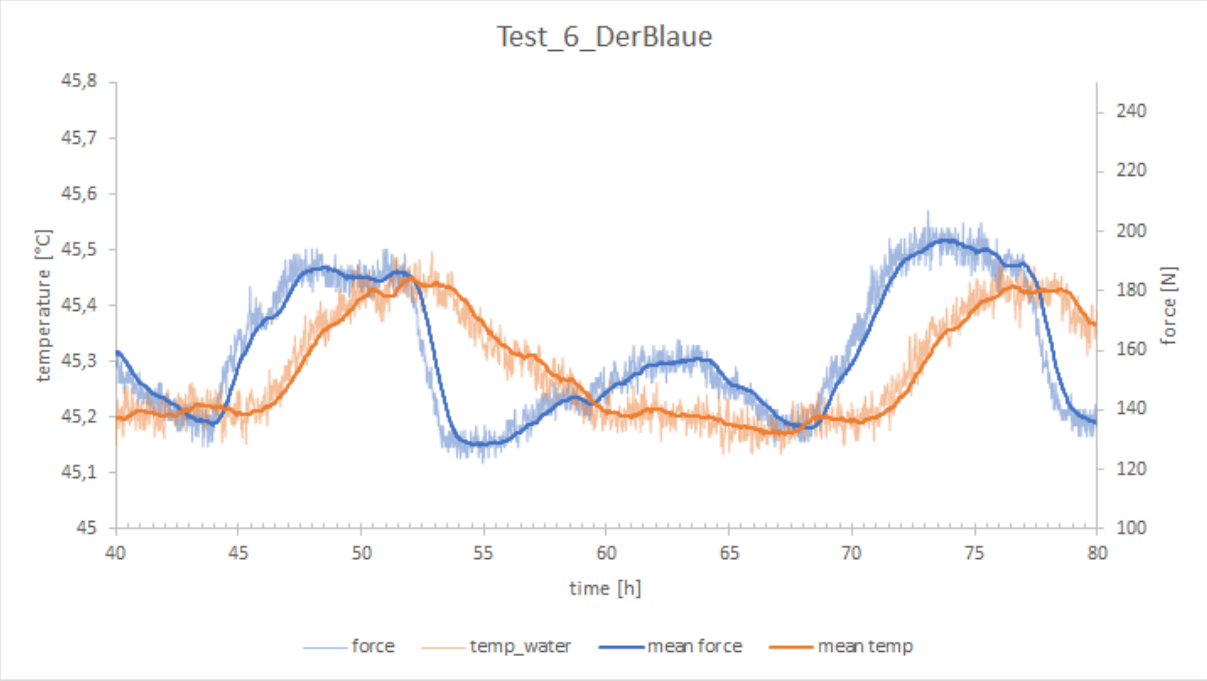

Fig. 4.10: Force and temperature development close-up – test 2.6

Another limitation stems from the compliance of the system, influenced by the oscillating behavior of thermally induced forces, which intermittently pressurizes and relieves the sample. The consequences of this mechanism on the sample behavior remain uncertain, potentially leading to distortions in the results. This compliance aspect transforms what initially appears to be a rigid system into one that allows minimal expansions.

Furthermore, precise control of the water preheating temperature is challenging due to discrepancies between the oven settings and the actual temperature within the oven. This discrepancy arises from the oven temperature sensor placement near the edges, close to the thermocouples. The oven was not originally designed for the high-precision requirements of this experiment, and as a result, the initial hours of the experiments can suffer from result distortions.

Additionally, the entire setup, including the sample introduction process, requires manual handling. As a consequence, it is influenced by body temperature, room temperature, and the varying temperature conditions it is exposed to. These variations predominantly affect the initial stages of the experiment.

Another factor worth mentioning is the rubber seal located between the lower cap of the steel tube and the water reservoir. It exhibits slight movement at very low forces, which is assumed to contribute to the non-linear development at the beginning of the compliance diagram (figure 4.11). The arrangement of all elements connected to one another can also play a significant role, especially at low forces.

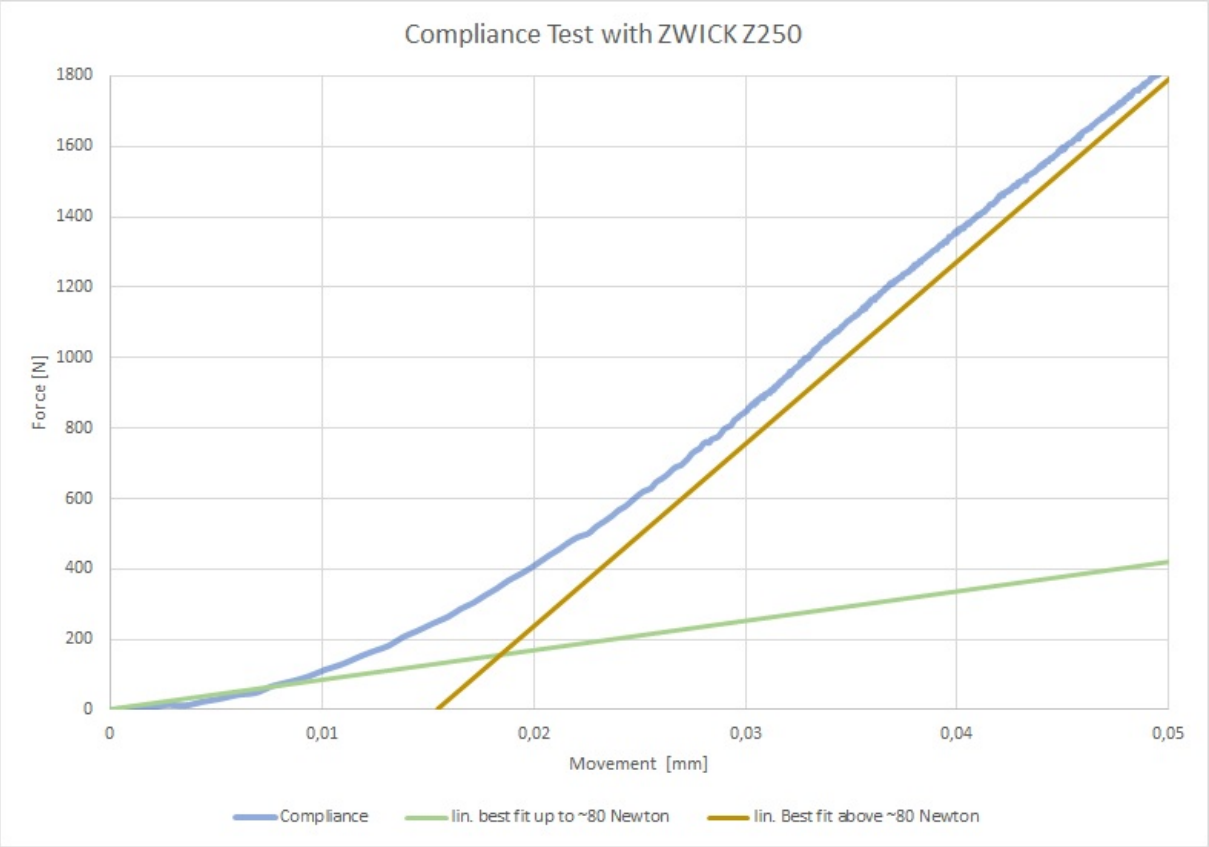

Fig. 4.11: First 1800 newton of compliance test

The potential deformation of the brick cutouts during the loading process is another concern. While it was not explicitly investigated whether these cutouts deform significantly in a water-saturated state, considering all the listed issues, it becomes evident that analyzing and interpreting the results is a complicated and error-prone task.

In summary, the results significance is critically influenced by a multitude of undesirable factors. What is unequivocal is that a certain level of force development occurs within the setup. However, the exact magnitude of this force and its temporal evolution remain unclear even after the experiments. It is apparent that the setup needs significant modifications to mitigate these issues and provide more precise answers to these questions.

Chapter 5

Conclusion

In conclusion, the development of a setup to measure the pressure of expansion in a confined environment, specifically applied to concrete, has been a complex journey with both successes and challenges. The motivation behind this study was rooted in addressing critical challenges in the construction industry, particularly in the context of recycling concrete. The focus on *internal Sulfate Attack (ISA)* within recycled concrete materials added a layer of complexity to the research, as this area had been relatively underexplored.

The experimental setup designed for these investigations, despite its intricacies, successfully facilitated controlled experiments to measure expansion pressure caused by secondary ettringite formation. The tests, such as Test 2.5 with *SupraCem45*, hydrated gypsum, and magnesium oxide, revealed valuable insights into the expansive behaviors of concrete mixtures. The recorded forces and their evolution over time shed light on the intricate relationship between temperature, material composition, and the measured pressure of expansion.

However, the significance of the obtained results is tempered by several problems and limitations inherent in the experimental setup. Fluctuations in temperature, both within the oven and in the surrounding environment, posed a considerable challenge. The compliance of the system, influenced by thermally induced forces, introduced uncertainties in quantifying the sample's behavior. Issues such as manual handling, rubber seal movements, and potential deformation of components further complicated the interpretation of results.

Despite these challenges, the experiments, especially Test 2.7 with hydrated *Der Blaue*, hydrated *Fondu*, and hydrated gypsum, provided valuable data on force development. The divergence between force and temperature profiles highlighted the need for precise control and measurement in future iterations of the experimental setup. The comprehensive analysis of each test, including a detailed examination of force and temperature trends, enabled a nuanced understanding of the complexities involved.

In essence, while the current setup yielded indicative results, its limitations underscore the necessity for significant modifications to enhance precision and reliability. Future iterations should address issues related to temperature control, system compliance, and manual handling to advance the understanding of pressure of expansion in a confined environment, especially concerning recycled concrete applications. The insights gained from this study, despite its limitations, lay the groundwork for further advancements in the development of setups for similar experiments and contribute to the broader goal of sustainable practices in the construction industry.

Bibliography

[1] H. Al Daffaie. "Expansion phenomena during internal sulfate attacks (ISA)". Diplomarbeit. Wien: Technische Universität Wien, 2022.

[2] P. C. Association. *Ettringite Formation and the Performance of Concrete*. Research rep. Portland Cement Association, 2014. 16 pp.

[3] R. Benedix. *Bauchemie für das Bachelor-Studium Modern – Kompetent – Kompakt*. Berlin: Springer Vieweg Wiesbaden, 2014. ISBN: 978-3-903311-35-0.

[4] L. Briendl, F. Mittermayr, R. Röck, F. R. Steindl, M. Sakoparnig, J. Juhart, F. Iranshahi, and I. Galan. "The hydration of fast setting spray binder versus (aluminum sulfate) accelerated OPC". In: *Materials and Structures* 55(2) (2022), p. 74. DOI: 10.1617/s11527-022-01907-x.

[5] K. L. S. C Famy, A. Atkinson, and A. R. Brough. "Influence of the storage conditions on the dimensional changes of heat-cured mortars". In: *Cement and Concrete Research* 31(5) (2001), pp. 795–803. DOI: 10.1016/S0008-8846(01)00480-X.

[6] M. Collepardi. "Ettringite Formation and Sulfate Attack on Concrete". In: (2001), pp. 21–28. DOI: 10.14359/10569.

[7] C. Colman, D. Bulteel, V. Thiéry, S. Rémond, F. Michel, and L. Courard. "Internal sulfate attack in mortars containing contaminated fine recycled concrete aggregates". In: *Construction and Building Materials* 272 (2021), p. 121851. DOI: 10.1016/j.conbuildmat.2020.121851.

[8] ConcreteTechnology. *Steam Curing of Concrete: Methods, and Advantages*. 2018. URL: https://test.theconstructor.org/concrete/steam-curing-concrete-methods-advantages/38837/ (visited on 08/10/2023).

[9] S. Diamond. "Delayed ettringite formation — Processes and problems". In: *Cement and Concrete Composites* 18(3) (1996), pp. 205–215. DOI: 10.1016/0958-9465(96)00017-0.

[10] J. Gao, Z. Yu, L. Song, and T. Wang. "Durability of concrete exposed to sulfate attack under flexural loading and drying–wetting cycles". In: *Construction and Building Materials* 39 (2013), pp. 33–38. DOI: 10.1016/j.conbuildmat.2012.05.033.

[11] A. Harrisson. "Constitution and Specification of Portland Cement". In: *Lea's Chemistry of Cement and Concrete, 5th Edition*. Ed. by P. Hewlett and M. Liska. Oxford: Butterworth-Heinemann, 2019, pp. 87–155. ISBN: 9780081007730.

[12] W. M. Haynes. *CRC Handbook of Chemistry and Physics, 96th Edition*. Boca Raton: CRC Press, 2015. ISBN: 978-1482260960.

[13] C. Hellmich. "Skriptum zur Vorlesung mit Übung aus Ingenieurmechanik Teil A - Vorlesungsteil". In: *Institut für Mechanik der Werkstoffe und Strukturen der Technischen Universität Wien* (2022).

[14] D. Herfort and D. Macphee. "Components in Portland Cement Clinker and Their Phase Relationships". In: *Lea's Chemistry of Cement and Concrete, 5th Edition*. Ed. by P. Hewlett and M. Liska. Oxford: Butterworth-Heinemann, 2019, pp. 57–86. ISBN: 9780081007730.

[15] HolcimGmbH. *Produktdatenblatt Der Blaue*. 2023. URL: https://www.holcim.at/fileadmin/Bibliothek/2_Zement/PDBL2023/PDBL_Der_Blaue_Mannersdorf.pdf (visited on 09/12/2023).

[16] J. Ideker. "Calcium Aluminate Cements". In: *Lea's Chemistry of Cement and Concrete, 5th Edition*. Ed. by P. Hewlett and M. Liska. Oxford: Butterworth-Heinemann, 2019, pp. 537–584. ISBN: 9780081007730.

[17] H. Jennings and J. Thomas. *Materials of Cement Science Primer*. Research rep. Infrastructure Technology Institute for TEA-21 funded projects, 2009. 98 pp.

[18] D. R. Katti and V. Shanmugasundaram. "Influence of swelling on the microstructure of expansive clays". In: *Can. Geothech J.* 38 (2001), pp. 175–182. DOI: 10.1139/cgj-38-1-175.

[19] J. Kollegger. "Skritum zur Betonbau Vorlesung". In: *Technische Universität Wien, Institut für Tragkonstruktionen* 10 (2018).

[20] J. li, F. Xie, G. Zhao, and L. Li. "Experimental and numerical investigation of cast-in-situ concrete under external sulfate attack and drying-wetting cycles". In: *Construction and Building Materials* 249(3) (2020), p. 118789. DOI: 10.1016/j.conbuildmat.2020.118789.

[21] X. Liu, P. Feng, W. Li, G. Geng, J. Huang, Y. Gao, S. Mu, and J. Hong. "Effects of pH on the nano/micro structure of calcium silicate hydrate (C-S-H) under sulfate attack". In: *Cement and Concrete Research* 140 (2021), p. 106306. DOI: 10.1016/j.cemconres.2020.106306.

[22] F. T. Madsen and M. Müller-Vonmoos. "The Swelling Behaviour of Clays". In: *Applied Clay Science* 4 (1989), pp. 153–156. DOI: 0169-1317/89/$03.50.

[23] P. Mehta. "Mechanism of Sulfate Attack on Portland Cement Concrete: Another Look." In: *Cement and Concrete Research* 13 (1983), pp. 401–406. DOI: 10.1016/0008-8846(83)90040-6.

[24] P. Mehta. "Scanning electron micrographic studies of ettringite formation". In: *Cement and Concrete Research* 6(2) (1976), pp. 169–182. DOI: 10.1016/0008-8846(76)90115-0.

[25] C. Meng, W. Li, L. Cai, X. Shi, and C. Jiang. "Experimental research on durability of high-performance synthetic fibers reinforced concrete: Resistance to sulfate attack and freezing-thawing". In: *Construction and Building Materials* 262(14) (2020), p. 120055. DOI: 10.1016/j.conbuildmat.2020.120055.

[26] S. Mindess. "Resistance of Concrete to Destructive Agencies". In: *Lea's Chemistry of Cement and Concrete, 5th Edition*. Ed. by P. Hewlett and M. Liska. Oxford: Butterworth-Heinemann, 2019, pp. 251–283. ISBN: 9780081007730.

[27] P. J. M. Monteiro. "Time to failure for concrete exposed to severe sulfate attack". In: *Cement and Concrete Research* 33(7) (2003), pp. 987–993. DOI: 10.1016/S0008-8846(02)01097-9.

[28] A. Neville. "The confused world of sulfate attack on concrete". In: *Construction and Building Materials* 34(8) (2004), pp. 1275–1296. DOI: 10.1016/j.cemconres.2004.04.004.

[29] I. Odler and M. Gasser. "Mechanism of Sulfate Expansion in Hydrated Portland Cement". In: *Journal of the American Ceramic Society* 71(11) (2005), pp. 1015–1020. DOI: 10.1111/j.1151-2916.1988.tb07573.x.

[30] N. Oikonomou. "Recycled concrete aggregates." In: *Cement and Concrete Composites* 27(2) (2005), pp. 315–318. DOI: 10.1016/j.cemconcomp.2004.02.020.

[31] I. Oliveira, S. H. Cavalaro, and A. Aguado. "New kinetic model to quantify the internal sulfate attack in concrete". In: *Cement and Concrete Research* 43 (2013), pp. 95–104. DOI: 10.1016/j.cemconres.2012.09.010.

[32] C. Ouyang, A. Nanni, and W. F. Chang. "Internal and external sources of sulfate ions in portland cement mortar: two types of chemical attack". In: *Cement and Concrete Research* 18(5) (1988), pp. 699–709. DOI: 10.1016/0008-8846(88)90092-0.

[33] K. Paine. "Physicochemical and Mechanical Properties of Portland Cements". In: *Lea's Chemistry of Cement and Concrete, 5th Edition*. Ed. by P. Hewlett and M. Liska. Oxford: Butterworth-Heinemann, 2019, pp. 285–339. ISBN: 9780081007730.

[34] S. S. Rehsi. "Magnesium Oxide in Portland Cement". In: *Advances in Cement Technology: Critical Reviews and Case Studies on Manufacturing, Quality Control, Optimization and Use*. Ed. by S. N. Ghosh. Oxford: Pergamon, 1983, pp. 467–483. ISBN: 9780080286709.

[35] G. W. Scherer. "Stress from Crystallization of Salt". In: *Cement and Concrete Research* 34(9) (2004), pp. 1613–1624. DOI: 10.1016/j.cemconres.2003.12.034.

[36] T. Schmidt, B. Lothenbach, M. Romer, K. L. Scrivener, D. Rentsch, and R. Figi. "A thermodynamic and experimental study of the conditions of thaumasite formation". In: *Cement and Concrete Research* 38(3) (2008), pp. 337–349. DOI: 10.1016/j.cemconres.2007.11.003.

[37] SchretterCie and GmbHCoKG. *SupraCem45 Schnellzement*. 2023. URL: https://www.schretter.tirol/pdf/SAP/TechnischesMerkblatt/TMB_SUPRACEM45.pdf (visited on 10/07/2023).

[38] I. Sims, J. Lay, and J. Ferrari. "Concrete Aggregates". In: *Lea's Chemistry of Cement and Concrete, 5th Edition*. Ed. by P. Hewlett and M. Liska. Oxford: Butterworth-Heinemann, 2019, pp. 699–778. ISBN: 9780081007730.

[39] P. del Strother. "Manufacture of Portland Cement". In: *Lea's Chemistry of Cement and Concrete, 5th Edition*. Ed. by P. Hewlett and M. Liska. Oxford: Butterworth-Heinemann, 2019, pp. 31–56. ISBN: 9780081007730.

[40] J. Tang, H. Cheng, Q. Zhang, and W. Chen. "Development of properties and microstructure of concrete with coral reef sand under sulphate attack and drying-wetting cycles". In: *Construction and Building Materials* 165(5) (2018), pp. 647–654. DOI: 10.1016/j.conbuildmat.2018.01.085.

[41] H. Taylor, C. Famy, and K. Scrivener. "Delayed ettringite formation". In: *Cement and Concrete Research* 31(5) (2001), pp. 683–693. DOI: 10.1016/S0008-8846(01)00466-5.

[42] S. Y. Teoh and V. N. Vangaveti. "Repeated hyperbaric exposure and glass ampoule safety". In: *Diving Hyperb Med.* 48(2) (2018), pp. 107–109. DOI: 10.28920/dhm48.2.107-109.

[43] M. Z. Y. Ting, K. S. Wong, M. E. Rahman, and S. J. Meheron. "Deterioration of marine concrete exposed to wetting-drying action". In: *Journal of Cleaner Production* 278 (2021), p. 123383. DOI: 10.1016/j.jclepro.2020.123383.

[44] K. Wang, J. Guo, H. Wu, and L. Yang. "Influence of dry-wet ratio on properties and microstructure of concrete under sulfate attack". In: *Construction and Building Materials* 263(3) (2020), p. 120635. DOI: 10.1016/j.conbuildmat.2020.120635.

[45] Y. Xiaotong, D. Chen, J.-r. Feng, and Y. Zhang. "Behavior of mortar exposed to different exposure conditions of sulfate attack." In: *Ocean Engineering* 157 (2018), pp. 1–12. DOI: 10.1016/j.oceaneng.2018.03.017.

[46] F. Xie, J. li, G. Zhao, and P. Zhou. "Experimental study on performance of cast-in-situ recycled aggregate concrete under different sulfate attack exposures". In: *Construction and Building Materials* 253(7) (2020), p. 119144. DOI: 10.1016/j.conbuildmat.2020.119144.

[47] G. Zhang, C. Wu, D. Hou, J. Yang, D. Sun, and X. Zhang. "Effect of environmental pH values on phase composition and microstructure of Portland cement paste under sulfate attack". In: *Composites Part B Engineering* 216(7) (2021), p. 108862. DOI: 10.1016/j.compositesb.2021.108862.

[48] H. Zhang, T. Ji, and H. Liu. "Performance evolution of recycled aggregate concrete (RAC) exposed to external sulfate attacks under full-soaking and dry-wet cycling conditions". In: *Construction and Building Materials* 248(10) (2020), p. 118675. DOI: 10.1016/j.conbuildmat.2020.118675.

[49] M. Zhang, J.-K. Chen, and Y. Lv. "Study on the expansion of concrete under attack of sulfate and sulfate–chloride ions". In: *Construction and Building Materials* 39(3) (2013), pp. 26–32. DOI: 10.1016/j.conbuildmat.2012.05.003.

[50] G. Zhao, J. li, M. Shi, and H. Fan. "Degradation mechanisms of cast-in-situ concrete subjected to internal-external combined sulfate attack". In: *Construction and Building Materials* 248 (2020), p. 118683. DOI: 10.1016/j.conbuildmat.2020.118683.

[51] G. Zhao, M. Shi, J. Cui, and J. li. "Degradation of cast-in-situ concrete subjected to sulphate-chloride combined attack". In: *Construction and Building Materials* 241(1) (2020), p. 117995. DOI: 10.1016/j.conbuildmat.2019.117995.

List of Figures

List of Tables